JHEP

Published for SISSA by Springer

Received: August 19, 2014
Revised: November 17, 2014
Accepted: November 22, 2014
Published: December 4, 2014

$h \to Z\gamma$ in the complex two Higgs doublet model

Duarte Fontes,[a] **J.C. Romão**[a] **and João P. Silva**[a,b,1]

[a] *Centro de Física Teórica de Partículas (CFTP), Instituto Superior Técnico, Universidade de Lisboa, 1049-001 Lisboa, Portugal*

[b] *Instituto Superior de Engenharia de Lisboa – ISEL, 1959-007 Lisboa, Portugal*

E-mail: duartefontes@tecnico.ulisboa.pt, jorge.romao@tecnico.ulisboa.pt, jpsilva@cftp.ist.utl.pt

Abstract: The latest LHC data confirmed the existence of a Higgs-like particle and made interesting measurements on its decays into $\gamma\gamma$, ZZ^*, WW^*, $\tau^+\tau^-$, and $b\bar{b}$. It is expected that a decay into $Z\gamma$ might be measured at the next LHC round, for which there already exists an upper bound. The Higgs-like particle could be a mixture of scalar with a relatively large component of pseudoscalar. We compute the decay of such a mixed state into $Z\gamma$, and we study its properties in the context of the complex two Higgs doublet model, analysing the effect of the current measurements on the four versions of this model. We show that a measurement of the $h \to Z\gamma$ rate at a level consistent with the SM can be used to place interesting constraints on the pseudoscalar component. We also comment on the issue of a wrong sign Yukawa coupling for the bottom in Type II models.

Keywords: Higgs Physics, Beyond Standard Model

ArXiv ePrint: 1408.2534

[1] Corresponding author.

doi:10.1007/JHEP12(2014)043

Contents

JHEP12(2014)043

1 Introduction

The ATLAS [1] and CMS [2] experiments at LHC have detected a particle with properties closely resembling those of the SM Higgs, in the decay channels $\gamma\gamma$, ZZ^*, WW^*, and $\tau^+\tau^-$, with errors of order 20%. Decays into $b\bar{b}$ are only detected at LHC and the Tevatron in connection with the associated Vh production mechanism, with errors of order 50% [3, 4]. Up-to-date LHC results can be found in refs. [5, 6].

The discovery of $pp \to h \to \gamma\gamma$ can be seen as the poster child of quantum field theory: the dominating production through gluon-gluon fusion occurs at one loop; and so does the decay into $\gamma\gamma$. Recently, ATLAS [7] and CMS [8] have reported on the search for another loop-decay, $h \to Z\gamma$, finding upper bounds of order ten times the SM expectation at the 95% confidence level. This is expected to be the next interesting channel to be measured in the upcoming LHC run.

As the newfound particle is further probed, there are two interesting questions that will be considered: i) is the new particle purely scalar, or does it have some pseudoscalar component?; ii) how many scalars are there? On the first issue, we know from the existence of $h \to VV$ that h cannot be purely pseudoscalar (henceforth, $V = W, Z$). There are some experimental bounds on the likelihood that the 125 GeV particle is a pure pseudoscalar [9, 10], but we are interested here in the possibility that the 125 GeV state is a mixture of scalar and pseudo-scalar components. On the second issue, although there have been some experimental fluctuations, there is currently no sign of another scalar. However, the limits are rather loose and the possibility remains that there are further scalar, including charged, that have evaded detection because its couplings are not too large. For example, in two Higgs doublet models, the fact that the observed scalar has couplings to two vector bosons in line with SM expectations forces the couplings of the heavier scalar to two vector bosons to be small.

The main objectives of this article are two-pronged. Firstly, we discuss the production and decays of a spin zero state which is a mixture of scalar and pseudoscalar, with special emphasis on a detailed discussion $h \to Z\gamma$. The details are contained in the appendices. Secondly, we analyze the current bounds on the complex two Higgs doublet model (C2HDM), where the lightest Higgs is in general a mixture of scalar and pseudoscalar.

The article is organized as follows. In section 2 we summarize the C2HDM and introduce our notation. In section 3 we discuss, in turn, current constraints and future reach on the four types of flavour couplings (Type I, Type II, Lepton Specific, and Flipped). As far as we know, this is the first update on the first two types, and the first discussion of the Lepton Specific and Flipped models to use the latest Run 1 data from LHC. In particular, we also discuss the effect of future experiments, and what might be learned from $h \to Z\gamma$ at LHC's Run 2. In section 4, we discuss the possibility that the scalar component of the $h_1 b\bar{b}$ coupling has a sign opposite to the SM. We relate this with the situation in the real 2HDM, which has received recent interest. In section 5, we comment briefly on the constraints from electric dipole moments. Finally, we draw our conclusions in section 6.

For completeness we collect in the appendices all the expressions needed for the production and decay of a Higgs boson which has a mixture of scalar and pseudo-scalar com-

JHEP12(2014)043

ponents; this includes the neutral scalars of the most general 2HDM. In particular, the expressions for the one loop decays are given in a form that can be useful for other models with a more general Higgs boson sector than the SM. We also compare our results with those that can be found in the literature.

2 The complex two Higgs doublet model

We consider a model with two Higgs doublets, ϕ_1 and ϕ_2, with the Z_2 symmetry $\phi_1 \to \phi_1, \phi_2 \to -\phi_2$ violated softly. The Higgs potential can be written as [11]

$$\begin{aligned} V_H = {} & m_{11}^2|\phi_1|^2 + m_{22}^2|\phi_2|^2 - m_{12}^2\,\phi_1^\dagger\phi_2 - (m_{12}^2)^*\,\phi_2^\dagger\phi_1 \\ & + \frac{\lambda_1}{2}|\phi_1|^4 + \frac{\lambda_2}{2}|\phi_2|^4 + \lambda_3|\phi_1|^2|\phi_2|^2 + \lambda_4\,(\phi_1^\dagger\phi_2)\,(\phi_2^\dagger\phi_1) \\ & + \frac{\lambda_5}{2}(\phi_1^\dagger\phi_2)^2 + \frac{\lambda_5^*}{2}(\phi_2^\dagger\phi_1)^2. \end{aligned} \tag{2.1}$$

Hermiticity implies that all couplings are real, except m_{12}^2 and λ_5. If $\arg(\lambda_5) \neq 2\arg(m_{12}^2)$, then the phases cannot be removed. This is known as the complex two Higgs doublet model (C2HDM), and has been studies extensively in[1] refs. [12–20]. If $\arg(\lambda_5) = 2\arg(m_{12}^2)$, then we can choose a basis where m_{12}^2 and λ_5 become real and, if the vacuum expectation values (vev) of ϕ_1 and ϕ_2 are also real, we talk about the real 2HDM. Henceforth, it is implicit that the C2HDM and the real 2HDM have a softly broken Z_2 symmetry.

With a suitable basis choice, we can take the vevs real:

$$\langle\phi_1\rangle = v_1/\sqrt{2}, \qquad \langle\phi_2\rangle = v_2/\sqrt{2}, \tag{2.2}$$

and write the scalar doublets as

$$\phi_1 = \begin{pmatrix} \varphi_1^+ \\ \frac{1}{\sqrt{2}}(v_1 + \eta_1 + i\chi_1) \end{pmatrix}, \qquad \phi_2 = \begin{pmatrix} \varphi_2^+ \\ \frac{1}{\sqrt{2}}(v_2 + \eta_2 + i\chi_2) \end{pmatrix}. \tag{2.3}$$

With this convention, $v = \sqrt{v_1^2 + v_2^2} = (\sqrt{2}G_\mu)^{-1/2} = 246\,\text{GeV}$, and the stationarity conditions become

$$\begin{aligned} -2\,m_{11}^2 &= -\text{Re}\left(m_{12}^2\right)\frac{v_2}{v_1} + \lambda_1\,v_1^2 + \lambda_{345}\,v_2^2, \\ -2\,m_{22}^2 &= -\text{Re}\left(m_{12}^2\right)\frac{v_1}{v_2} + \lambda_2\,v_2^2 + \lambda_{345}\,v_1^2, \\ 2\,\text{Im}\left(m_{12}^2\right) &= v_1 v_2\,\text{Im}\left(\lambda_5\right), \end{aligned} \tag{2.4}$$

where $\lambda_{345} = \lambda_3 + \lambda_4 + \text{Re}\left(\lambda_5\right)$.

We can now transform the fields into the Higgs basis by [21, 22]

$$\begin{pmatrix} H_1 \\ H_2 \end{pmatrix} = \begin{pmatrix} c_\beta & s_\beta \\ -s_\beta & c_\beta \end{pmatrix}\begin{pmatrix} \phi_1 \\ \phi_2 \end{pmatrix}, \tag{2.5}$$

[1] Our notation differs from theirs, and agrees with [11], in that $2m_{11}^2 = -m_{11}^2(\text{theirs})$, $2m_{22}^2 = -m_{22}^2(\text{theirs})$, and $2m_{12}^2 = m_{12}^2(\text{theirs})$.

JHEP12(2014)043

where $\tan\beta = v_2/v_1$, $c_\beta = \cos\beta$, and $s_\beta = \sin\beta$. The Higgs basis was introduced [21, 22] such that the second Higgs does not get a vev:

$$H_1 = \begin{pmatrix} G^+ \\ \frac{1}{\sqrt{2}}(v + H^0 + iG^0) \end{pmatrix}, \qquad H_2 = \begin{pmatrix} H^+ \\ \frac{1}{\sqrt{2}}(R_2 + iI_2) \end{pmatrix}. \tag{2.6}$$

In this basis, G^+ and G^0 are massless and, in the unitary gauge, will become the longitudinal components of W^+ and Z^0, respectively. There remains a charged pair $H^\pm$ with mass $m_{H^\pm}$.

In the usual notation for the C2HDM, $\eta_3 = I_2$, and the three neutral components mix into the neutral mass eigenstates through

$$\begin{pmatrix} h_1 \\ h_2 \\ h_3 \end{pmatrix} = R \begin{pmatrix} \eta_1 \\ \eta_2 \\ \eta_3 \end{pmatrix}. \tag{2.7}$$

The orthogonal matrix R diagonalizes the neutral mass matrix

$$\left(\mathcal{M}^2\right)_{ij} = \frac{\partial^2 V_H}{\partial\eta_i\,\partial\eta_j}, \tag{2.8}$$

through

$$R\,\mathcal{M}^2\,R^T = \text{diag}\left(m_1^2, m_2^2, m_3^2\right), \tag{2.9}$$

where $m_1 \leq m_2 \leq m_3$ are the masses of the neutral Higgs particles. The matrix R can be parametrized as [14]

$$R = \begin{pmatrix} c_1c_2 & s_1c_2 & s_2 \\ -(c_1s_2s_3 + s_1c_3) & c_1c_3 - s_1s_2s_3 & c_2s_3 \\ -c_1s_2c_3 + s_1s_3 & -(c_1s_3 + s_1s_2c_3) & c_2c_3 \end{pmatrix} \tag{2.10}$$

where $s_i = \sin\alpha_i$ and $c_i = \cos\alpha_i$ $(i = 1, 2, 3)$. Without loss of generality, the angles may be restricted to [14]

$$-\pi/2 < \alpha_1 \leq \pi/2, \qquad -\pi/2 < \alpha_2 \leq \pi/2, \qquad 0 \leq \alpha_3 \leq \pi/2. \tag{2.11}$$

The relation between the Higgs basis and the mass basis is

$$\begin{pmatrix} \eta_1 \\ \eta_2 \\ \eta_3 \end{pmatrix} = R_H \begin{pmatrix} H^0 \\ R_2 \\ I_2 \end{pmatrix} = \begin{pmatrix} c_\beta & -s_\beta & 0 \\ s_\beta & c_\beta & 0 \\ 0 & 0 & 1 \end{pmatrix} \begin{pmatrix} H^0 \\ R_2 \\ I_2 \end{pmatrix}. \tag{2.12}$$

Thus

$$\begin{pmatrix} h_1 \\ h_2 \\ h_3 \end{pmatrix} = R \begin{pmatrix} \eta_1 \\ \eta_2 \\ \eta_3 \end{pmatrix} = R\,R_H \begin{pmatrix} H^0 \\ R_2 \\ I_2 \end{pmatrix}. \tag{2.13}$$

The computation of the bounds from the oblique radiative corrections in eqs. (388) and (393) of ref. [11] requires the matrix $T = R_H^T R^T$ in eq. (381) of ref. [11].

JHEP12(2014)043

Given an arbitrary relative phase, the Higgs potential in eq. (2.1) has 9 independent parameters. We follow ref. [15], and trade these for v and for the 8 input parameters β, $m_{H^\pm}$, α_1, α_2, α_3, m_1, m_2, and $\mathrm{Re}(m_{12}^2)$. With this choice, m_3 is given by

$$m_3^2 = \frac{m_1^2\, R_{13}(R_{12}\tan\beta - R_{11}) + m_2^2\, R_{23}(R_{22}\tan\beta - R_{21})}{R_{33}(R_{31} - R_{32}\tan\beta)}. \tag{2.14}$$

Of course, we are only interested in those cases where $m_3^2 > 0$, and, due to our mass ordering, $m_3^2 > m_2^2 > m_1^2$. This places constraints on the relevant parameter space.

The Higgs potential in eq. (2.1) can be reconstructed through

$$\begin{aligned}
v^2\,\lambda_1 &= -\frac{1}{\cos^2\beta}\left[-m_1^2\, c_1^2 c_2^2 - m_2^2(c_3 s_1 + c_1 s_2 s_3)^2 - m_3^2\,(c_1 c_3 s_2 - s_1 s_3)^2 + \mu^2\,\sin^2\beta\right], \\
v^2\,\lambda_2 &= -\frac{1}{\sin^2\beta}\left[-m_1^2\, s_1^2 c_2^2 - m_2^2\,(c_1 c_3 - s_1 s_2 s_3)^2 - m_3^2\,(c_3 s_1 s_2 + c_1 s_3)^2 + \mu^2\,\cos^2\beta\right], \\
v^2\,\lambda_3 &= \frac{1}{\sin\beta\cos\beta}\left[\left(m_1^2\, c_2^2 + m_2^2\,(s_2^2 s_3^2 - c_3^2) + m_3^2\,(s_2^2 c_3^2 - s_3^2)\right) c_1 s_1\right. \\
&\qquad \left. + (m_3^2 - m_2^2)(c_1^2 - s_1^2) s_2 c_3 s_3\right] - \mu^2 + 2m_{H^\pm}^2\,, \\
v^2\,\lambda_4 &= m_1^2\, s_2^2 + (m_2^2\, s_3^2 + m_3^2\, c_3^2) c_2^2 + \mu^2 - 2m_{H^\pm}^2, \\
v^2\,\mathrm{Re}(\lambda_5) &= -m_1^2\, s_2^2 - (m_2^2\, s_3^2 + m_3^2\, c_3^2) c_2^2 + \mu^2, \\
v^2\,\mathrm{Im}(\lambda_5) &= \frac{2}{\sin\beta} c_2\left[(-m_1^2 + m_2^2\, s_3^2 + m_3^2\, c_3^2) c_1 s_2 + (m_2^2 - m_3^2) s_1 s_3 c_3\right],
\end{aligned} \tag{2.15}$$

where

$$\mu^2 = \frac{v^2}{v_1\, v_2}\,\mathrm{Re}(m_{12}^2). \tag{2.16}$$

We have checked that, using eq. (2.14), we reproduce the results in eq. (B.1) of ref. [19].

To compute the decays of the lightest Higgs we need the couplings $h_1 VV$ ($V = W, Z$), $h_1 H^+ H^-$, and $h_1 \bar{f} f$ for some fermion f. These can be obtained from the Higgs potential, the covariant derivatives, and the Yukawa potential, respectively. As shown in ref. [20], the $h_1 VV$ and $h_1 H^+ H^-$ can be written, respectively, as in eqs. (A.3) and (A.2), with

$$C = c_\beta R_{11} + s_\beta R_{12} = \cos(\alpha_2)\,\cos(\alpha_1 - \beta), \tag{2.17}$$

and

$$-\lambda = c_\beta\left[s_\beta^2 \lambda_{145} + c_\beta^2 \lambda_3\right] R_{11} + s_\beta\left[c_\beta^2 \lambda_{245} + s_\beta^2 \lambda_3\right] R_{12} + s_\beta c_\beta\,\mathrm{Im}(\lambda_5)\, R_{13}, \tag{2.18}$$

where $\lambda_{145} = \lambda_1 - \lambda_4 - \mathrm{Re}(\lambda_5)$ and $\lambda_{245} = \lambda_2 - \lambda_4 - \mathrm{Re}(\lambda_5)$. In order to preclude flavour changing interactions with the neutral Higgs, each fermion sector must couple to only one Higgs. In the usual notation, up-type quarks couple to ϕ_2, so there are four possibilities according to the couplings of down-type quarks and charged leptons. In Type I (Type II) both couple to ϕ_2 (ϕ_1). In Lepton Specific (Flipped), down-type quarks couple to ϕ_2 (ϕ_1), while charged leptons couple to ϕ_1 (ϕ_2). The result can be written as in eq. (A.1), with the coefficients $a + ib\gamma_5$ given in table 1.

Looking back at eqs. (2.7) and (2.10), we realize that $|s_2|$ measures the pseudoscalar component of the lightest neutral scalar, h_1. Indeed, when $s_2 = 0$, the pseudoscalar η_3

JHEP12(2014)043

	Type I	Type II	Lepton Specific	Flipped
Up	$\frac{R_{12}}{s_\beta} - ic_\beta \frac{R_{13}}{s_\beta}\gamma_5$	$\frac{R_{12}}{s_\beta} - ic_\beta \frac{R_{13}}{s_\beta}\gamma_5$	$\frac{R_{12}}{s_\beta} - ic_\beta \frac{R_{13}}{s_\beta}\gamma_5$	$\frac{R_{12}}{s_\beta} - ic_\beta \frac{R_{13}}{s_\beta}\gamma_5$
Down	$\frac{R_{12}}{s_\beta} + ic_\beta \frac{R_{13}}{s_\beta}\gamma_5$	$\frac{R_{11}}{c_\beta} - is_\beta \frac{R_{13}}{c_\beta}\gamma_5$	$\frac{R_{12}}{s_\beta} + ic_\beta \frac{R_{13}}{s_\beta}\gamma_5$	$\frac{R_{11}}{c_\beta} - is_\beta \frac{R_{13}}{c_\beta}\gamma_5$
Leptons	$\frac{R_{12}}{s_\beta} + ic_\beta \frac{R_{13}}{s_\beta}\gamma_5$	$\frac{R_{11}}{c_\beta} - is_\beta \frac{R_{13}}{c_\beta}\gamma_5$	$\frac{R_{11}}{c_\beta} - is_\beta \frac{R_{13}}{c_\beta}\gamma_5$	$\frac{R_{12}}{s_\beta} + ic_\beta \frac{R_{13}}{s_\beta}\gamma_5$

Table 1. Couplings of the fermions to the lightest scalar, h_1, in the form $a + ib\gamma_5$ of eq. (A.1).

does not contribute to h_1, while, when $c_2 = 0$ only the pseudoscalar η_3 contributes to h_1. That is,

$$|s_2| = 0 \implies h_1 \text{ is a pure scalar,} \tag{2.19}$$

$$|s_2| = 1 \implies h_1 \text{ is a pure pseudoscalar.} \tag{2.20}$$

This is confirmed by the form of the various couplings. In fact, the h_1VV coupling C in eq. (2.17) vanishes when $|s_2| = 1$, in agreement with the absence of a pseudoscalar coupling with a vector boson/anti-boson pair. Similarly, when $|s_2| = 1$ the only term in λ which survives is the term proportional to $\mathrm{Im}(\lambda_5)$ in eq. (2.18). This is consistent with the fact that a pseudoscalar can only couple to H^+H^- if there is explicit CP violation in the Higgs potential. Finally, when $s_2 = 0$, all b coefficients in table 1 (multiplying $i\gamma_5$) vanish, and h_1 couples to fermions as a pure scalar. Similarly, when $|s_2| = 1$, all a coefficients in table 1 vanish, and h_1 couples to fermions as a pure pseudoscalar.

3 Simulation procedure and results

For our fit procedure, we generate points in parameter space with $m_1 = 125\,\mathrm{GeV}$, the angles $\alpha_{1,2,3}$ within the intervals of eq. (2.11), $1 \leq \tan\beta \leq 30$, $m_1 \leq m_2 \leq 900\,\mathrm{GeV}$, $-(900\,\mathrm{GeV})^2 \leq m_{12}^2 \leq (900\,\mathrm{GeV})^2$, and $340\,\mathrm{GeV} \leq m_{H^\pm} \leq 900\,\mathrm{GeV}$ (Type II and Flipped), or $100\,\mathrm{GeV} \leq m_{H^\pm} \leq 900\,\mathrm{GeV}$ (Type I and Lepton Specific).

The ranges for $m_{H^\pm}$ and $\tan\beta$ where chosen to comply with the constraints from $Z \to b\bar{b}$, $b \to s\gamma$, and other B-Physics results. The constraints are basically the same in the complex and real 2HDM because the charged Higgs couplings to fermions coincide — see, for example, appendix C of [19]. In Type II and Flipped, $Z \to b\bar{b}$ implies $\tan\beta \gtrsim 1$ while $b \to s\gamma$ excludes values of $m_{H^\pm}$ below 360 GeV, at the 95% confidence level, with only a very mild dependence on $\tan\beta$ [23–26]. In Type I and Lepton Specific, $\tan\beta \gtrsim 1$ still holds, but $m_{H^\pm}$ can be as low as ~ 90GeV, even after the LHC results on $pp \to t\bar{t}$ with decay into $H^+\bar{b}$ [27, 28]. The ranges we have chosen for $m_{H^\pm}$ and $\tan\beta$ conform to rather conservative bounds from these and other B-Physics experiments, and, for comparison purposes, were taken to coincide with the constraints in refs. [29, 30], in the CP conservative limit.

Given a set of input parameters, m_3^2 is obtained from eq. (2.14). With our conventions, one should only take points where $m_3^2 > m_2^2$. Then, we derive the parameters of the scalar potential from eqs. (2.15), and maintain those points which provide a bounded from

JHEP12(2014)043

channel	ATLAS	CMS
$\mu_{\gamma\gamma}$	$1.57^{+0.33}_{-0.28}$	1.13 ± 0.24
μ_{WW}	$1.00^{+0.32}_{-0.29}$	0.83 ± 0.21
μ_{ZZ}	$1.44^{+0.40}_{-0.35}$	1.00 ± 0.29
$\mu_{\tau^+\tau^-}$	$1.4^{+0.5}_{-0.4}$	0.91 ± 0.27
$\mu_{b\bar{b}}$	$0.2^{+0.7}_{-0.6}$	0.93 ± 0.49

Table 2. Experimental results presented by ATLAS and CMS at ICHEP2014.

below solution [31], conforming to perturbative unitarity [32–34], and the oblique radiative parameters S, T, U [35, 36]. After implementing this algorithm, we have a collection of possible C2HDM data points.

We generate the rates for all channels, including all production mechanisms. We use the expressions in the appendices, and utilize HIGLU [37] at NNLO for $gg \to h$ (gluon fusion), SusHi [38] at NNLO for $b\bar{b} \to h$, and ref. [39] for Vh (associated production), $t\bar{t}h$, and $VV \to h$ (vector boson fusion). The expressions for the decay rates are obtained in the appendices. In particular, $h \to Z\gamma$ is explained in great detail in C and D.2, for a generic scalar/pseudoscalar mixed state h. Finally, we compute the ratio of rates

$$\mu_f = \frac{\sigma^{\rm 2HDM}(pp \to h)}{\sigma^{\rm SM}(pp \to h)} \frac{\Gamma^{\rm 2HDM}[h \to f]}{\Gamma^{\rm SM}[h \to f]} \frac{\Gamma^{\rm SM}[h \to \text{all}]}{\Gamma^{\rm 2HDM}[h \to \text{all}]}\,, \tag{3.1}$$

where σ is the cross section for Higgs production, $\Gamma[h \to f]$ is the decay width into the final state f, and $\Gamma[h \to \text{all}]$ is h's total width. The ratios μ_f can then be compared with those quoted by the experimental collaborations. For definiteness, our discussions will be based on the ATLAS [40] and CMS [41] results presented in the plenary talks at ICHEP2014, which we summarize in table 2. Notice that the errors are still important; combining ATLAS and CMS would lead to errors of order 20% in VV, $\gamma\gamma$, and slightly larger in $\tau^+\tau^-$. On the other hand, the errors on $b\bar{b}$, which is only detected in associated production, are of order 50%. In particular, ATLAS excludes the SM $\mu_{\gamma\gamma} = 1$ ($\mu_{ZZ} = 1$) at 2-σ (1-σ), while CMS is within 1-σ of the SM on all channels.

We note that the ranges we adopt already evade current effects of heavy scalars and LHC bounds. The reason is easy to understand. On the one hand, LHC bounds place the h_1VV coupling close to the alignment limit. This implies that h_2VV and h_3VV are heavily suppressed, and rather light h_2 and h_3 are possible which are virtually undetected in VV final states. On the other hand, the LHC bounds on $h_{2,3} \to \gamma\gamma$ are very weak because the corresponding branching ratio decreases very steeply due to the opening of new channels, as the scalar mass increases.

3.1 Type I model

To study the effect of current experimental bounds on the pseudoscalar content of the 125 GeV Higgs, we follow ref. [20] and study three sets of points: points where the h_1 is mainly scalar, with $|s_2| < 0.1$ (in green/light-grey in the simulation figures to be shown

JHEP12(2014)043

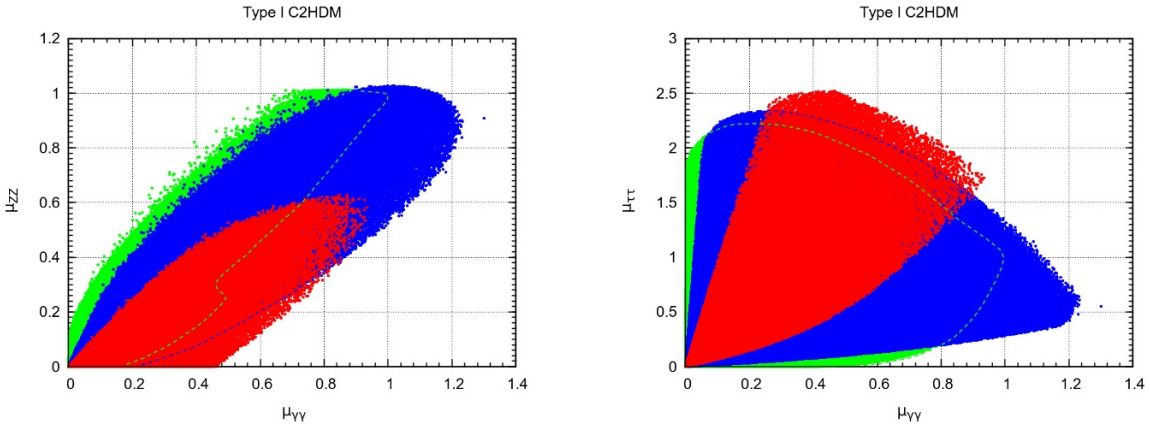

Figure 1. Left panel: results in the μ_{ZZ} - $\mu_{\gamma\gamma}$ plane (left panel) and in the $\mu_{\tau^+\tau^-}$ - $\mu_{\gamma\gamma}$ plane (right panel) for the Type I C2HDM. The points in green/light-grey, blue/black, and red/dark-grey correspond to $|s_2| < 0.1$, $0.45 < |s_2| < 0.55$, and $|s_2| > 0.85$, respectively.

below); points where the h_1 is mainly pseudoscalar, with $|s_2| > 0.85$ (in red/dark-grey in the simulation figures to be shown below); points where the h_1 is a almost even mix of scalar and pseudoscalar, with $0.45 < |s_2| < 0.55$ (in blue/black in the simulation figures to be shown below).

To compare with current experiments, all figures in this article will be drawn for processes at 8 TeV, except were noted otherwise. The exceptions are figures drawn at 14 TeV, designed to foresee future experimental reaches. Nevertheless, we have checked that there are very small differences between 8 TeV and 14 TeV, for the figures that interest us. As explained in [30], this is due to the fact that the ratio between the dominant and sub-dominant gluon fusion production mechanisms (which, in the two Higgs doublet model, can be relevant with both top and bottom quarks in the loop) remains very similar as one changes from 8 TeV to 14 TeV in our HIGLU simulations.

Our results for μ_{ZZ} versus $\mu_{\gamma\gamma}$ are shown in the left panel of figure 1. This can be compared with figure 1 of ref. [20]. We get qualitatively the same results, meaning that $|s_2| > 0.85$ is excluded by CMS at 1-σ. Also, larger values of $\mu_{\gamma\gamma}$ are obtained with $0.45 < |s_2| < 0.55$ than with $|s_2| < 0.1$. Thus, a putative future result of, for example, $\mu_{\gamma\gamma} = 1.3 \pm 0.1$ (consistent with the current ATLAS bound) would imply that the Higgs found at LHC has comparable scalar and pseudoscalar components. Notice from the left panel of figure 1 that this would be consistent with $\mu_{ZZ} \sim 0.9$ but less so with $\mu_{ZZ} \sim 1$.

On the right panel of figure 1, we show our results in the $\mu_{\gamma\gamma} - \mu_{\tau^+\tau^-}$ plane. This can be compared with figure 2 of ref. [20] which shows $\mu_{b\bar{b}}$ considering, as we correct below, all production channels. There is qualitative agreement, but there are subtle differences, because we are using the latest version of HIGLU [37], and, eventually, different PDF's and energy scales. The difference is apparent when plotting $\mu_{\tau^+\tau^-}$ as a function of $\tan\beta$. As shown in ref. [30], $\mu_{\tau^+\tau^-}$ is very sensitive to the production rates (and, thus, should be interpreted with care), while $\mu_{\gamma\gamma}$ and $\mu_{Z\gamma}$ are not. With this caution, we find that values

JHEP12(2014)043

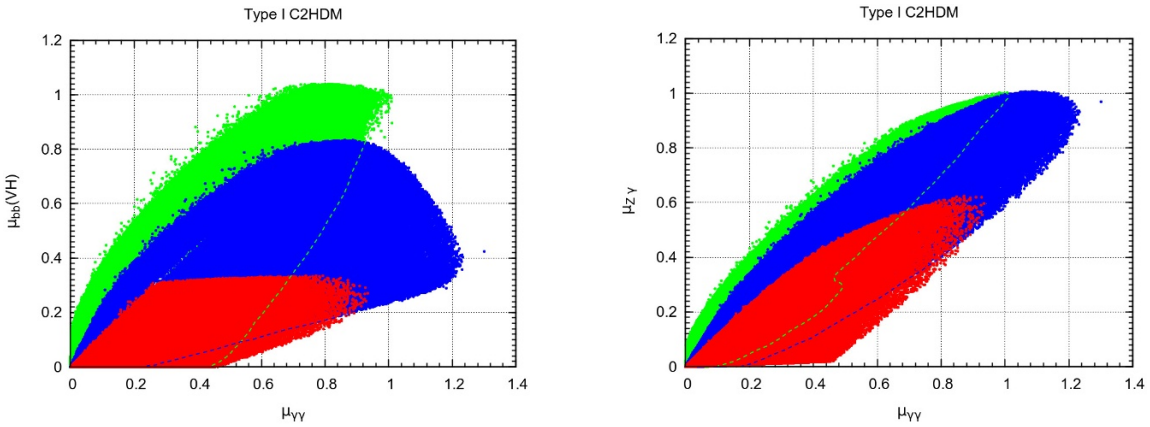

Figure 2. Left panel: results in the $\mu_{b\bar{b}}(Vh)$ - $\mu_{\gamma\gamma}$ plane (left panel) and in the $\mu_{Z\gamma}$ - $\mu_{\gamma\gamma}$ plane (right panel) for the Type I C2HDM. The points in green/light-grey, blue/black, and red/dark-grey correspond to $|s_2| < 0.1$, $0.45 < |s_2| < 0.55$, and $|s_2| > 0.85$, respectively.

as large as $\mu_{\tau^+\tau^-} \sim 2$ are allowed. If one requires $\mu_{\gamma\gamma} \sim 1$, then $\mu_{\tau^+\tau^-}$ lies roughly between 0.4 and 1.4.

In ref. [20], $\mu_{b\bar{b}}$ was calculated using all production channels. Here we use exclusively the Vh production mechanism that allows detection at LHC. Our results are shown on the left panel of figure 2. In the Type I model, $\mu_{b\bar{b}}(Vh) \lesssim 1.1$ for all values of $|s_2|$, and $\mu_{b\bar{b}}(Vh) \lesssim 0.35$ for $|s_2| > 0.85$. Thus, we learn that CMS excludes again $|s_2| > 0.85$ at 1-σ (recall that even the SM ZZ and $\gamma\gamma$ are outside ATLAS' 1-σ intervals), and a good measurement of $\mu_{b\bar{b}}(Vh)$ will be useful in ruling out large pseudoscalar components.

Now we turn to one of the main motivations for this work. The right panel of figure 2 shows our results in the $\mu_{\gamma\gamma} - \mu_{Z\gamma}$ plane. We notice that large pseudoscalar components (large $|s_2|$) imply small values for $\mu_{Z\gamma}$. There are two points to stress. First, there is a strong correlation between $\mu_{Z\gamma}$ and $\mu_{\gamma\gamma}$, even when all values of s_2 are taken into account. Second, that correlation is partly connected with s_2. This can be seen in the blue/black regions of figures 3, where we see that large values of $\mu_{Z\gamma}$ and $\mu_{\gamma\gamma}$ are only possible around $s_2 \sim 0$ and h_1 with a large scalar component. In contrast, a large pseudoscalar component implies very small values for both $\mu_{Z\gamma}$ and $\mu_{\gamma\gamma}$. As a result, a value of $\mu_{Z\gamma} \sim 1$ would be very efficient in ruling out a large pseudoscalar component. Figures 3 also show in red/dark-grey (cyan/light-grey) the allowed regions if we assume that the measurements of μ_{VV} at 14 TeV will center around unity with a 20% (5%) error. The VV constraint implies that $\mu_{\gamma\gamma}$ and $\mu_{Z\gamma}$ are expected to lie close to their SM value in the C2HDM and that $|\alpha_2|$ should lie below 50 degrees. A similar analysis of the impact of VV, shows that α_3 can take any value and that $|\alpha_1|$ should be larger than about 60 degrees.

JHEP12(2014)043

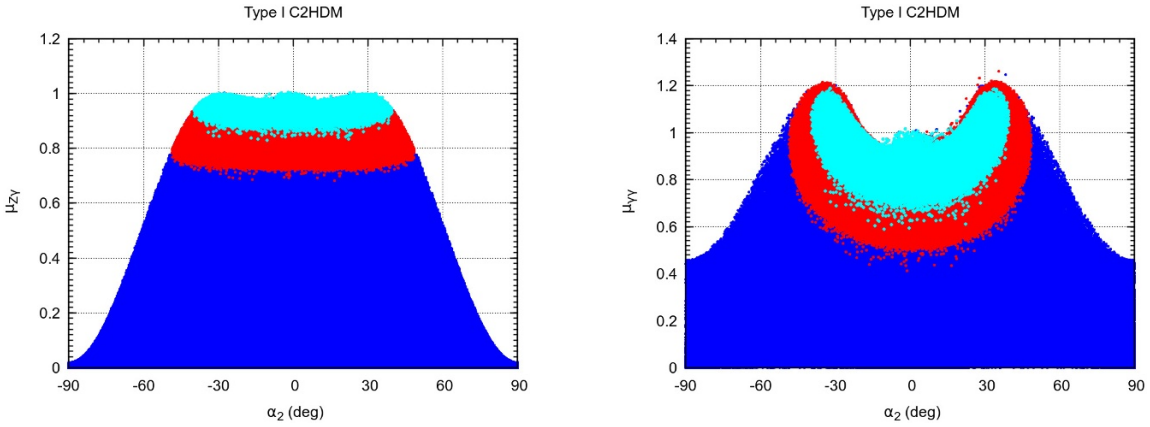

Figure 3. Figures of $\mu_{Z\gamma}$ ($\mu_{\gamma\gamma}$) on the left (right) panel, as a function of s_2. The points in red/dark-grey (cyan/light-grey) where chosen to obey $\mu_{VV} = 1$ within 20% (5%). These figures have been drawn for 14 TeV.

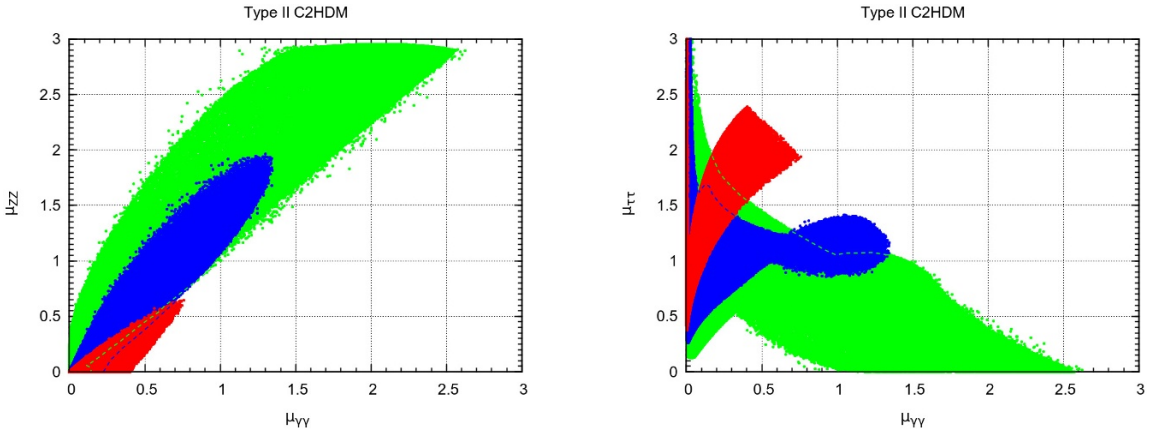

Figure 4. Left panel: results in the μ_{ZZ} - $\mu_{\gamma\gamma}$ plane (left panel) and in the $\mu_{\tau^+\tau^-}$ - $\mu_{\gamma\gamma}$ plane (right panel) for the Type II C2HDM. The points in green/light-grey, blue/black, and red/dark-grey correspond to $|s_2| < 0.1$, $0.45 < |s_2| < 0.55$, and $|s_2| > 0.85$, respectively.

3.2 Type II model

The results obtained in Type II for μ_{ZZ} versus $\mu_{\gamma\gamma}$ are shown in the left panel of figure 4. In this model, values as large as $\mu_{\gamma\gamma} \sim 2.5$ and $\mu_{ZZ} \sim 3$ are allowed for small values of s_2. In contrast, $|s_2| > 0.85$ forces both to be smaller than 0.8. This means that even the high central values quoted by ATLAS are consistent with a Type II C2HDM where h_1 has a dominant scalar component. In fact, one can find $s_2 < 0.1$ but also a few $0.45 < |s_2| < 0.55$ points within the ATLAS and CMS 1-σ bounds. As occurred in Type I, both experiments exclude a large pseudoscalar component ($|s_2| > 0.85$) at more than 1-σ. However, in contrast to Type I, here the largest values of $\mu_{\gamma\gamma}$ occur for $s_2 < 0.1$ and not for $0.45 < |s_2| < 0.55$. That is, in Type I a large value ($\mu_{\gamma\gamma} \sim 1.2$) favors a comparable scalar/pseudoscalar mix, while in Type II a large value (here, $\mu_{\gamma\gamma} \geq 1.2$) favors a pure scalar.

JHEP12(2014)043

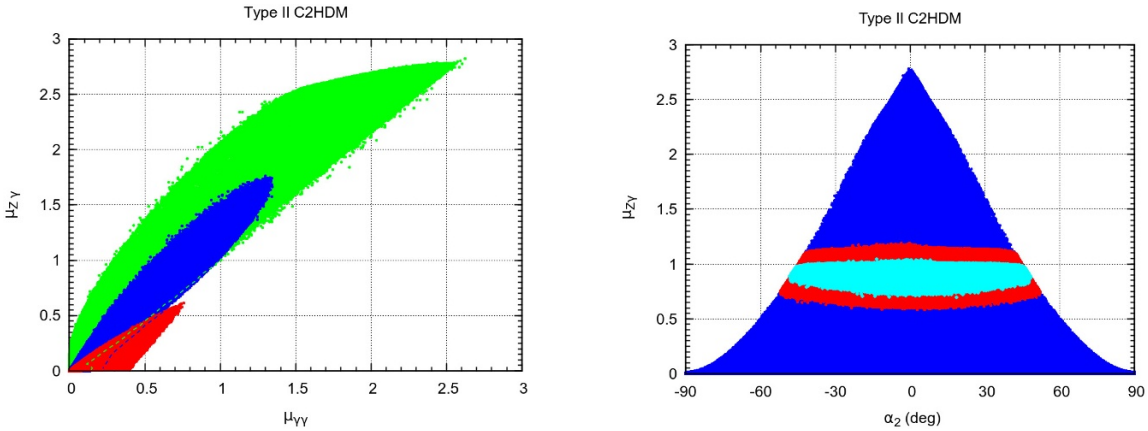

Figure 5. Left panel: type II results in the $\mu_{Z\gamma}$ - $\mu_{\gamma\gamma}$ plane. The points in green/light-grey, blue/black, and red/dark-grey correspond to $|s_2| < 0.1$, $0.45 < |s_2| < 0.55$, and $|s_2| > 0.85$, respectively. Right panel: type II predictions in the $\mu_{Z\gamma}$ - s_2 plane. The points in red/dark-grey (cyan/light-grey) where chosen to obey $\mu_{VV} = 1$ within 20% (5%). This figure has been draw at 14 TeV.

Curiously, the situation is the reverse when one considers $\mu_{\tau^+\tau^-}$, which we show on the right panel of figure 4. For example, for $\mu_{\gamma\gamma} \sim 1$, a value of $\mu_{\tau^+\tau^-} \sim 1.3$ favors an even scalar/pseudoscalar mix over the pure scalar solution. In contrast, $|s_2|$ is less easily constrained from $\mu_{b\bar{b}}(Vh)$, although $\mu_{b\bar{b}}(Vh) \gtrsim 0.4$ rules out $|s_2| > 0.85$. Looking at the various channels, both CMS and ATLAS rule out $|s_2| > 0.85$ by more than 2-σ in Type II C2HDM. Better measurements of $\gamma\gamma$, $\tau^+\tau^-$, and $b\bar{b}(Vh)$ will be instrumental in determining s_2.

Next, we consider the simulations for $Z\gamma$, shown in on the left panel of figure 5. Large values for $\mu_{Z\gamma}$ are possible for small $|s_2|$. Comparing with the right panel of figure 2 we see that in Type II much larger values of $\mu_{Z\gamma}$ (and of $\mu_{\gamma\gamma}$) are allowed, but that there is still a strong correlation between the two which, again, is partly due to s_2. This is shown on the right panel of figure 5, where we see that large values of $\mu_{Z\gamma}$ require large values of μ_{VV} and correspond to an almost pure scalar. Measurements of μ_{VV} within 20% of unity, force $\mu_{Z\gamma} \sim 1$ and require $|\alpha_2| \lesssim 50$ degrees. This puts a further bound on a large pseudoscalar component.

3.3 Lepton specific model

In this case, the results for μ_{ZZ} and $\mu_{b\bar{b}}(Vh)$ versus $\mu_{\gamma\gamma}$ are very similar to those presented on the left panels of figures 1 and 2 for Type I, respectively. The same holds for $\mu_{Z\gamma}$, shown on the right panel of figure 2. Minute differences are as follows. Close to $\mu_{\gamma\gamma} \sim 1$, one can get slightly larger values for μ_{ZZ}, up to approximately 1.1. Conversely, $\mu_{\gamma\gamma} \lesssim 1.1$ here, while $\mu_{\gamma\gamma} \lesssim 1.3$ in Type I. Here, as in Type I, $|s_2| > 0.85$ forces $\mu_{b\bar{b}}(Vh) < 0.3$. Thus, a good measurement of $\mu_{b\bar{b}}(Vh)$ will be instrumental in ruling out large pseudoscalar components.

As expected, the situation for $\mu_{\tau^+\tau^-}$ differs, as shown in figure 6. A large pseudoscalar component ($|s_2| > 0.85$) forces $\mu_{\tau^+\tau^-} > 1.2$ when $\mu_{\gamma\gamma} > 0.1$. These values are ruled out by

JHEP12(2014)043

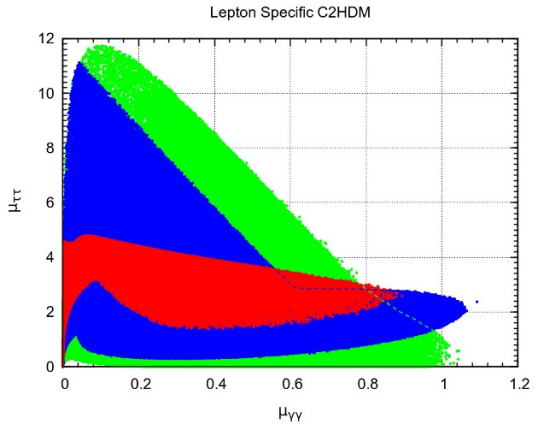

Figure 6. Lepton Specific simulations in the $\mu_{\tau^+\tau^-}$ - $\mu_{\gamma\gamma}$ plane. The points in green/light-grey, blue/black, and red/dark-grey correspond to $|s_2| < 0.1$, $0.45 < |s_2| < 0.55$, and $|s_2| > 0.85$, respectively.

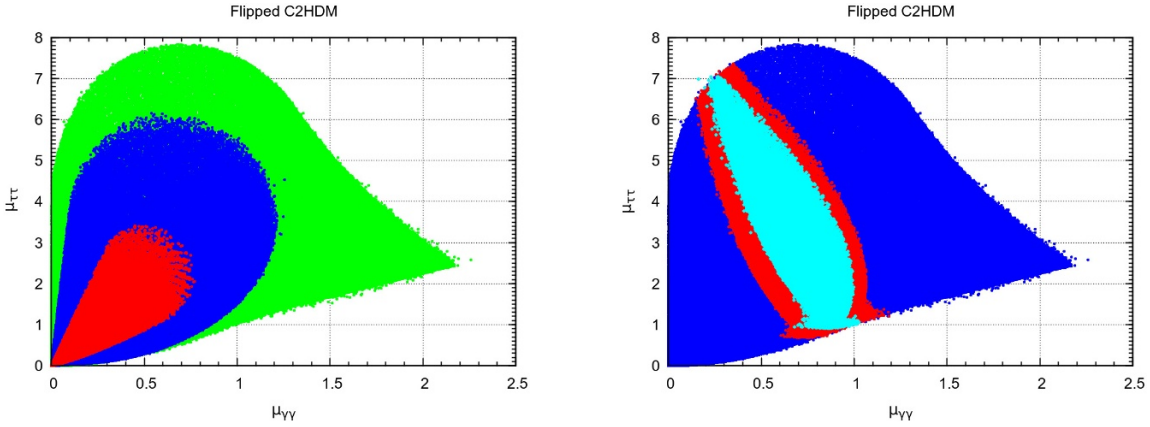

Figure 7. Left panel: flipped model results in the $\mu_{\tau^+\tau^-}$ - $\mu_{\gamma\gamma}$ plane. The points in green/light-grey, blue/black, and red/dark-grey correspond to $|s_2| < 0.1$, $0.45 < |s_2| < 0.55$, and $|s_2| > 0.85$, respectively. Right panel: same as left, except that all values for s_2 are included as blue/black points. Also shown as red/dark-grey (cyan/light-grey) are those points which obey $\mu_{VV} = 1$ within 20% (5%).

CMS at 1-σ. ATLAS, on the other hand, is barely consistent with these values for $\mu_{\tau^+\tau^-}$, but rules out this model (and the SM) in $\mu_{\gamma\gamma}$ at 1-σ.

3.4 Flipped model

The results for $\mu_{\gamma\gamma}$, μ_{ZZ}, $\mu_{b\bar{b}}(Vh)$, and $\mu_{Z\gamma}$ in this model, are similar to those for Type II. Slight differences are as follows. Here $\mu_{\gamma\gamma}$ (μ_{ZZ}, $\mu_{\gamma\gamma}$) can only be as large as 2.2 (2.5, 2.4), while one could achieve 2.5 (2.9, 2.8) in Type II. The situation for $\mu_{b\bar{b}}(Vh)$ is virtually the same. In particular, $|s_2| > 0.85$ is ruled out at 1-σ by both ATLAS and CMS.

The situation is very different for $\mu_{\tau^+\tau^-}$, as shown on the left panel of figure 7. Notice that one can find points as large as $\mu_{\tau^+\tau^-} = 7.5$ for reasonable values of $\mu_{\gamma\gamma} \sim 1$.

JHEP12(2014)043

As mentioned in ref. [30], constraints on μ_{VV} have a very strong impact on predictions in Type II and Flipped models, which have a simple trigonometric interpretation. One might wonder whether large values for $\mu_{\tau^+\tau^-}$ are consistent with μ_{VV}. This is shown on the right panel of figure 7: the red/dark-grey (cyan/light-grey) are those points which obey $\mu_{VV} = 1$ within 20% (5%). We see that large values of $\mu_{\tau^+\tau^-}$ are still allowed. Thus, $\mu_{\tau^+\tau^-}$ will have an enormous impact in probing the Flipped C2HDM.

4 Wrong sign $h_1 b\bar{b}$ couplings in Type II C2HDM

Recently there has been great interest in probing the wrong sign $hb\bar{b}$ couplings, in the context of the real 2HDM [29, 30, 42–44]. Here we discuss for the first time this issue in the context of the Type II C2HDM.

In the Type II real 2HDM the coupling of $h_1 = h$ with the down-type quarks and the charged leptons may be written as $m_f k_D/v$, where m_f is the mass of the appropriate fermion, and

$$k_D = -\frac{\sin\alpha}{\cos\beta}\,. \tag{4.1}$$

Here, α is the angle mixing the two CP even scalar components into a light scalar h and a heavy scalar H. Thus, $\sin\alpha$ negative (positive) corresponds to the (opposite of the) SM sign for k_D in Type II. Given the experimental lower bound on $\tan\beta$, the coupling to the up-type quarks in Type I and Type II, as well as the coupling to the down-type quarks in Type I cannot have the wrong sign. The regions of Type II with right and wrong sign are disjoint in that the current measurements of μ_{VV} force $\sin(\beta-\alpha) \sim +1$ when $k_D > 0$ and $\sin(\beta+\alpha) \sim +1$ when $k_D < 0$ (dubbed, the wrong-sign solution). To be precise and independent of the phase conventions leading to the usual choices for the ranges of α, one should talk about $Ck_D > 0$ as the right sign solution and $Ck_D < 0$ as the wrong sign solution, where $C = \sin(\beta-\alpha)$ is the hVV couplings in the real 2HDM, divided by the $h_{\rm SM}VV$ coupling in the SM.[2]

The situation is rather different in the C2HDM because, according to eq. (A.1), there are two couplings of h_1 with the fermions: the scalar-like coupling a, and the pseudoscalar-like coupling b. We follow the spirit of refs. [20, 29] and assume that experiments have obtained the SM values for μ_{ZZ}, $\mu_{\gamma\gamma}$, and $\mu_{\tau^+\tau^-}$ within 20%. Denoting by $\mathrm{sgn}(C)$ the sign of C, we show in figure 8 a simulation in the $\mathrm{sgn}(C)\,\sin(\alpha_1 - \pi/2)$-$\tan\beta$ plane. This reduces to the well known $\sin\alpha$-$\tan\beta$ plane of the real 2HDM, with the usual angle conventions, when we take the limit $|s_2| \to 0$ and $|s_3| \to 0$. In cyan/light-grey we show the points which pass $\mu_{VV} = 1.0 \pm 0.2$; in blue/black the points that also satisfy $|s_2|, |s_3| < 0.1$; and in red/dark-grey the points that satisfy $|s_2|, |s_3| < 0.05$. The left panel of figure 8 should be compared with the right panel, obtained in the real 2HDM. The left leg of that panel corresponds to $\sin(\beta-\alpha) \sim 1$ and the right sign solution, while the right leg corresponds to $\sin(\beta+\alpha) \sim 1$ and the wrong sign solution. We see that, for generic s_2 and s_3, the two regions are continuously connected. In contrast, when $|s_2|, |s_3| < 0.05$, we tend to the disjoint solutions of the real 2HDM, as we should.

[2] Rui Santos, private communication.

JHEP12(2014)043

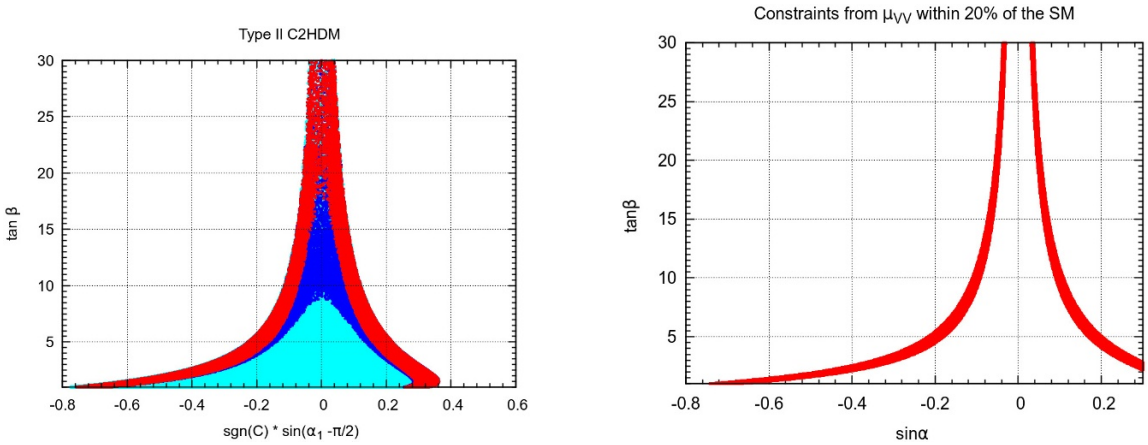

Figure 8. On the left (right) panel, we show the results of the simulation of Type II C2HDM (real 2HDM) on the $\mathrm{sgn}(C)\,\sin(\alpha_1 - \pi/2)$-$\tan\beta$ ($\sin\alpha$-$\tan\beta$) plane. On the left panel, in cyan/light-grey we show all points obeying $\mu_{VV} = 1.0 \pm 0.2$; in blue/black the points that satisfy in addition $|s_2|$, $|s_3| < 0.1$; and in red/dark-grey the points that satisfy $|s_2|$, $|s_3| < 0.05$.

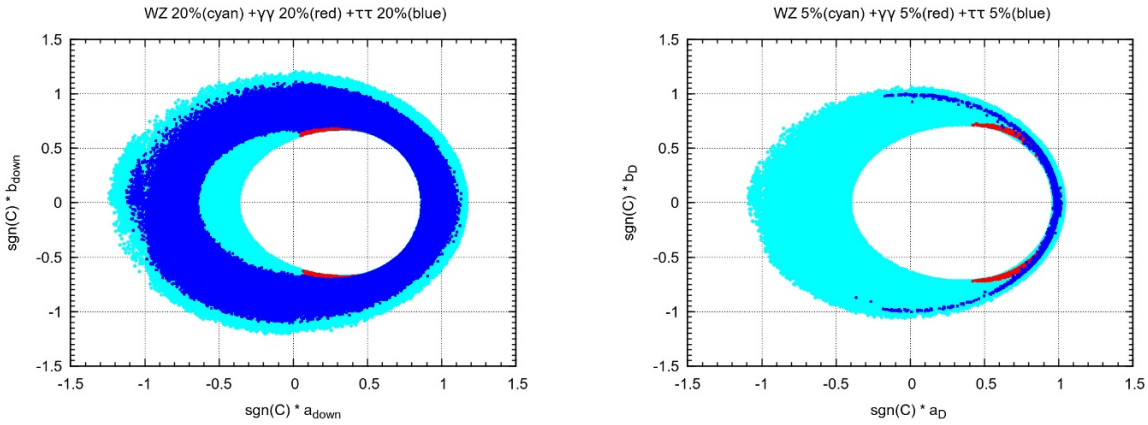

Figure 9. Results of the simulation of Type II C2HDM on the $\mathrm{sgn}(C)\,a_D$-$\mathrm{sgn}(C)\,b_D$ plane of scalar-pseudoscalar couplings of $h_1 b\bar{b}$. On the left panel (right panel) we assume that the measurements come from current data at 8 TeV (prospective data at 14 TeV) and are made within 20% (5%) of the SM. Constraints from μ_{VV} are in cyan/light-grey, from $\mu_{\gamma\gamma}$ are in red/dark-grey, and from $\mu_{\tau^+\tau^-}$ are in blue/black.

The constraints on the $\mathrm{sgn}(C)\,a_D$-$\mathrm{sgn}(C)\,b_D$ plane are shown on the left panel of figure 9. We see that $\mathrm{sgn}(C)\,a_D$ can have both signs (as it could in the CP conserving limit, where $a_D = k_D$), and so can $\mathrm{sgn}(C)\,b_D$. Moreover, these different regions are continuously connected. In the C2HDM there is still a very large region of either negative sign permitted. The situation will be altered if future measurements fix μ_{VV}, $\mu_{\gamma\gamma}$, and $\mu_{\tau^+\tau^-}$ to within 5% of the SM, as shown on the right panel of figure 9. In that case, there will be almost no region with $\mathrm{sgn}(C)\,a_D < 0$. This is consistent with the disappearance of the negative k_D region in the real Type II 2HDM when the measurements reach the 5% level [29]. However, in the C2HDM some points with $\mathrm{sgn}(C)\,a_D \sim -0.4$ are allowed, if one also has a large pseudoscalar coupling $\mathrm{sgn}(C)\,b_D \sim -0.8$.

JHEP12(2014)043

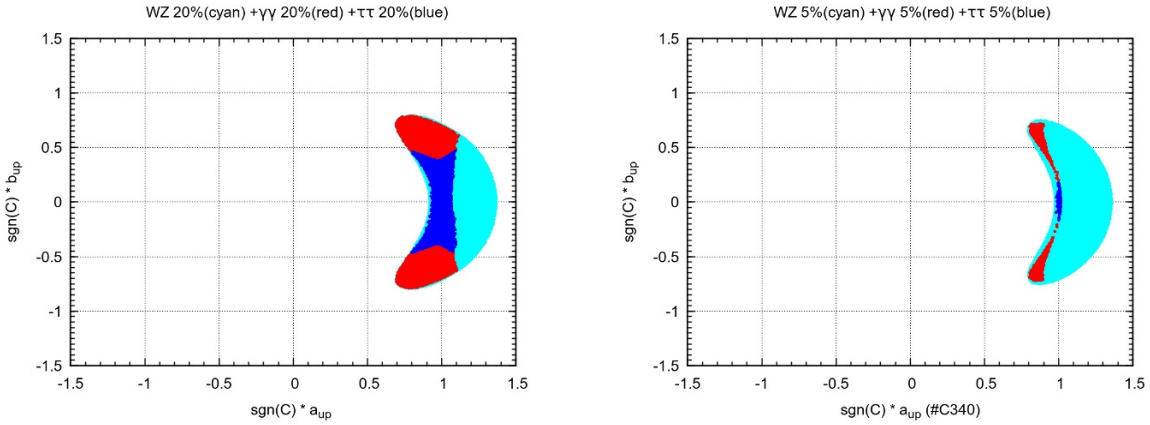

Figure 10. Results of the simulation of Type II C2HDM on the $\mathrm{sgn}(C)\, a_U$-$\mathrm{sgn}(C)\, b_U$ plane of scalar-pseudoscalar couplings of $h_1 t\bar{t}$. On the left panel (right panel) we assume that the measurements come from current data at 8 TeV (prospective data at 14 TeV) and are made within 20% (5%) of the SM. Constraints from μ_{VV} are in cyan/light-grey, from $\mu_{\gamma\gamma}$ are in red/dark-grey, and from $\mu_{\tau^+\tau^-}$ are in blue/black.

In the real 2HDM, the lower bound $\tan\beta > 1$ implies that the coupling of $ht\bar{t}$ must be positive. In the C2HDM, it is still true that the scalar like coupling $\mathrm{sgn}(C)\, a_U$ must be positive, but the pseudoscalar like $\mathrm{sgn}(C)\, b_U$ can have either sign. This is illustrated in figure 10, for measurements within 20% (left panel) and 5% (right panel) of the SM. Notice that $\mu_{\gamma\gamma}$ forces the figure into the outer rim, and that adding $\mu_{\tau^+\tau^-}$ forces $\mathrm{sgn}(C)\, a_U \sim 1$ and $|b_U| \lesssim 0.2$. This shows that the line of blue/black points which one guesses on the right panel of figure 9 corresponds to $\mathrm{sgn}(C)\, a_U \sim 1$.

A final point of interest concerns the effect on delayed decoupling. In the real 2HDM, wrong sign solutions exist only with $k_D \sim -1$. In fact, as explained in [30], a rather simple trigonometric explanation justifies that a 20% bound on μ_{VV} implies an even better determination of $\sin^2(\beta-\alpha)$ for a given $\tan\beta$.[3] As pointed out in ref. [29], this solution exists if and only if the charged Higgs loop gives a contribution of order 10% to $h \to \gamma\gamma$, due to the fact that the hH^+H^- coupling λ — see eq. (A.2) — exhibits a non-decoupling with the charged Higgs mass, curtailed only by the requirements of unitarity. In figure 11, we show what happens to λ as a function of a_D multiplied by the sign of C. On the left panel of figure 11, the points in cyan/light-grey pass $\mu_{VV} = 1$ within 20%. The points in red/dark-grey pass this constraint and, in addition, $\mu_{\tau^+\tau^-} = 1$ within 20%. The points in blue/black pass the previous two constraints and, in addition, $\mu_{\gamma\gamma} = 1$ within 20%. These simulations were made at 8 TeV to allow a feeling for the current constraints. The colour code on the right panel are: cyan/light-grey points pass $\mu_{VV} = 1$ within 5%; red/dark-grey points pass in addition $\mu_{\gamma\gamma} = 1$ within 5%; blue/black points pass the previous two constraints and, in addition, $\mu_{\gamma\gamma} = 1$ within 5%. These prospective simulations have been drawn at 14 TeV.

[3]For example, for $\tan\beta = 10$, a 20% bound around $\mu_{VV} \sim 1$ implies a determination of $\sin^2(\beta-\alpha)$ to better than 0.5%.

JHEP12(2014)043

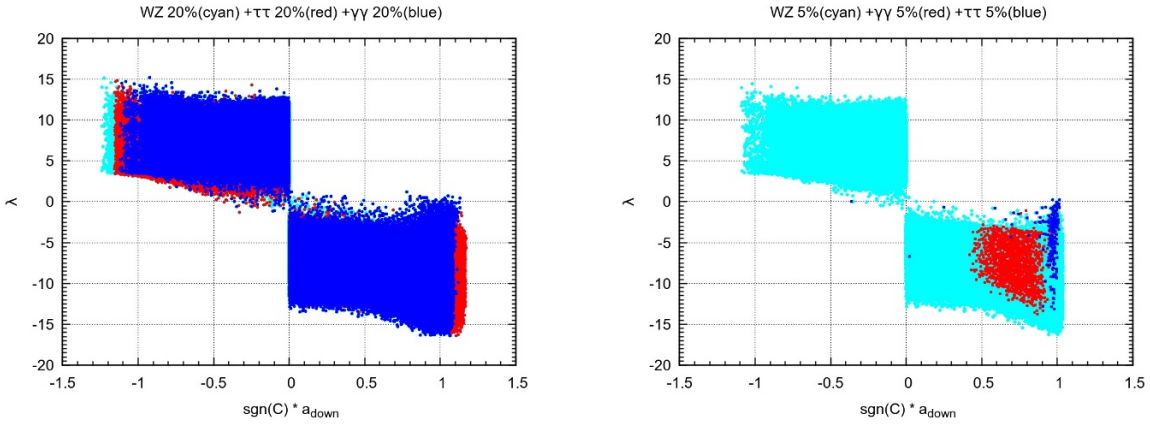

Figure 11. Results of the simulation of Type II C2HDM on the sign(C) a_D-λ plane. On the left panel (right panel) we assume that the measurements come from current data at 8 TeV (prospective data at 14 TeV) and are made within 20% (5%) of the SM. Constraints from μ_{VV} are in cyan/light-grey; adding constraints from $\mu_{\tau^+\tau^-}$ ($\mu_{\gamma\gamma}$ at 5%) only the points in red/dar-grey survive; adding constraints from $\mu_{\gamma\gamma}$ ($\mu_{\tau^+\tau^-}$ at 5%) only the points in blue/black, survive.

From the left panel of figure 11, we see that in the C2HDM one can have any value for sign(C) a_D between around -1.1 and 1.05. This is different from the real 2HDM where $k_D \sim 1$ and $k_D \sim -1$ form two disjoint solutions. The difference, of course, is due to the fact that in the C2HDM there is a new pseudoscalar coupling b_D. But there is a similarity. Indeed, values of sign(C) $a_D \sim -1$ correspond to non-negligible values for λ, as seen on the left panel of figure 11. This is the analogous of the delayed decoupling found for $k_D \sim -1$ solutions found in the real 2HDM. The right panel of figure 11 shows again that a putative 5% future measurement around the SM to be made at 14 TeV will eliminate almost all the sign(C) $a_D < 0$ points.

5 Constraints from EDM

CP violation is constrained by bounds on the electric dipole moments (EDMs) of neutrons, atoms and molecules. The recent announcement by the ACME Collaboration [45] of improved bounds on the the electron EDM from their experiment with the ThO molecule has spurred renewed interest in the subject. Several analysis of EDM constraints in the 2HDM have appeared in the last few years [46–48], including two concerning specifically the C2HDM discussed in this article [49, 50]. Although using mainly specific choices for most parameters, ref. [50] finds that the strongest bounds on CP violation in the type I and Type II C2HDM come from the ThO experiment, with neutron EDM and Hg EDM relevant only in small regions of parameter space where there are cancelling contributions to the electron EDM.

The fact that there can be cancelling contributions from the three neutral scalars has been pointed out in ref. [49], and a simple explanation put forth in ref. [48]. The argument is as follows. The couplings of the scalar mass eigenstate h_k is as in eq. (A.1), with $h \to h_k$ and $a + ib\gamma_5 \to a_k + ib_k\gamma_5$, where a_k and b_k depend on the field type (up, down, charged-lepton), and on the model (Type I, Type II, Lepton specific and Flipped). For example,

JHEP12(2014)043

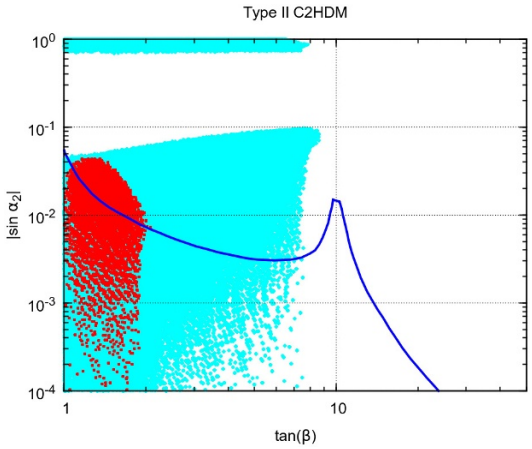

Figure 12. Results of the simulation of Type II C2HDM on the $|s_2|$, $\tan\beta$ plane. We assume masses consistent with figure 6 of ref. [50], which gives the electron EDM constraint, shown here in blue/black. Points that pass all theoretical constraints are shown in cyan/light-gray, while points that pass in addition μ_{VV} at 20% are shown in red/dar-grey.

in Type II

$$\begin{aligned} \text{up:} \qquad & a_k + i b_k \gamma 5 = \frac{R_{k2}}{s_\beta} - i c_\beta \frac{R_{k3}}{s_\beta} \gamma 5 \,, \\ \text{down:} \qquad & a_k + i b_k \gamma 5 = \frac{R_{k1}}{c_\beta} - i s_\beta \frac{R_{k3}}{c_\beta} \gamma 5 \,. \end{aligned} \tag{5.1}$$

CP violation involving neutral scalars and the up type quarks will thus be proportional to $a_k b_k \sim R_{k2} R_{k3}$, multiplied by some function of the mass of h_k. However, the orthogonality of R implies that

$$\sum_k a_k b_k \sim \sum_k R_{k2} R_{k3} = 0 \,. \tag{5.2}$$

This means that there is complete cancellation of the three contributions when the scalars are fully degenerate. Ref. [48] shows that the same happens in the decoupling regime. The same argument holds, of course, for the down type quarks and the charged leptons. As a result, one cannot assume dominance of the lightest scalar [48, 50]. In the C2HDM, CP violation in the charge Higgs interactions arises only from the CKM matrix. Charged Higgs appear in Barr-Zee type $H^\pm W^\mp \gamma$ contributions to the EDM.[4] Nevertheless, they give sub-dominant contributions to the electron EDM, as shown in figure 5 of ref. [50].

In figure 12, we show the constraints from LHC and from the electron EDM for Type II. In order to compare with figure 6 of ref. [50], we have taken $m_{H^\pm} \sim 420$GeV, $m_2 \sim 400$GeV, $m_3 \sim 450$GeV, and $\mathrm{Re}(m_{12}^2) \sim v^2 c_\beta s_\beta$. The set of points obtained after the theoretical constraints are shown in cyan/light-gray in figure 12. In red/dar-gray, we show those points that satisfy, in addition, μ_{VV} equal to unity, within 20%. Also shown, in blue/black, is the electron EDM constraint obtained from figure 6 of ref. [50]. For $\tan\beta \sim 1.5$, we see that $\mu_{VV} = 1.0 \pm 0.2$ allows for $|s_2| \sim 0.2$, while the electron EDM favours $|s_2| \lesssim 0.05$. We

[4] See, for example, figure 12 in ref. [50], and also ref. [51].

JHEP12(2014)043

note that this choice of masses and angles is barely allowed, and it would not pass a future $\mu_{\gamma\gamma} = 1.0 \pm 0.1$ measurement. We conclude that in the near future the constraints on the C2HDM will profit from an interplay between the LHC data and the electron EDM data, but that LHC's Run 2 will provide very relevant new constraints. The analysis of ref. [50] is restricted to a few mass choices. A full simulation of the EDM constraints on the C2HDM will be interesting, but lies beyond the scope of this work, and will be pursued elsewhere.

6 Conclusions

The 125 GeV particle found at LHC could have a pseudoscalar component. We discuss in detail the decay of a mixed scalar/pseudoscalar state into $Z\gamma$, which will be probed in the next LHC run. We consider the constraints that current experiments impose on the four versions of the C2HDM and discuss the prospects of future bounds, including $h \to Z\gamma$. This provides an update of Type I and Type II, and the first discussion of current constraints on the Lepton Specific and Flipped C2HDM.

In the C2HDM, the parameter s_2 measures the pseudoscalar content, with $s_2 = 0$ ($|s_2| = 1$) corresponding to a pure scalar (pseudoscalar). The fact that ATLAS has a rather large central value for $\mu_{\gamma\gamma}$ places strong limits on C2HDM, but it also disfavours the SM at 2-σ. But, even excluding this constraint, we find that current experiments already disfavor a large pseudoscalar component $|s_2| > 0.85$, at over 1-σ level in all C2HDM versions.

As for future experimental reaches, we find that in all types of C2HDM a better measurement of $\mu_{b\bar{b}}(Vh) \sim 1$ will exclude large values of the pseudoscalar component s_2. Similarly, a measurement of $\mu_{Z\gamma} \sim 1$ will also exclude a very large s_2 component. The Flipped C2HDM is special in that one can have $\mu_{\tau^+\tau^-} \sim 7$ and, thus, the $\tau^+\tau^-$ channel will be crucial in probing this model.

Further, we have discussed the possibility that the scalar component of the Type II C2HDM $h_1 q\bar{q}$ coupling (a) has a sign opposite to that in the SM. The fact that the C2HDM also has a pseudoscalar component of the $h_1 q\bar{q}$ coupling (b) gives more room for differences than are possible within the Type II real 2HDM. We found that the up quark coupling $\mathrm{sgn}(C)\, b_U$ can have either sign, while $\mathrm{sgn}(C)\, a_U$ must be positive. If future experiments yield μ_{VV}, $\mu_{\gamma\gamma}$, and $\mu_{\tau^+\tau^-}$ within 5% of the SM, then $\mathrm{sgn}(C)\, b_U$ can still have either sign, but $\mathrm{sgn}(C)\, a_U = 1$ to very high precision, corresponding to the limit $s_1 c_2 = s_\beta$. In contrast, current experiments allow for either sign of both $\mathrm{sgn}(C)\, a_D$ and $\mathrm{sgn}(C)\, b_D$, covering a rather large region. However, if future experiments yield μ_{VV}, $\mu_{\gamma\gamma}$, and $\mu_{\tau^+\tau^-}$ within 5% of the SM, then the region in the $\mathrm{sgn}(C)\, a_D$-$\mathrm{sgn}(C)\, b_D$ plane reduces to a line, with most points concentrated around $\mathrm{sgn}(C)\, a_D \sim 1$. Still, there are a few points with $\mathrm{sgn}(C)\, a_D \sim -0.4$, as long as $\mathrm{sgn}(C)\, b_D \sim -0.8$ is rather large. Finally we have discussed briefly the possible constraints on this model coming from the EDMs and their interplay with the future LHC's Run 2 data.

JHEP12(2014)043

A Production and decay rates

A.1 Lagrangian

The appendices contains the production and decay rates for a scalar particle with both scalar and pseudo-scalar components. We assume that the SM particles except the Higgs follow the usual lagrangian, that there are $H^\pm$ particles with the usual gauge-kinetic Lagrangian, and that the new scalar/pseudoscalar particle h has the following interactions:

$$\mathcal{L}_Y = -\left(\sqrt{2}G_\mu\right)^{\frac{1}{2}} m_f \, \bar{\psi}\,(a + ib\gamma_5)\,\psi\, h, \tag{A.1}$$

$$\mathcal{L}_{hH^+H^-} = \lambda\, v\, hH^+H^-, \tag{A.2}$$

$$\mathcal{L}_{hVV} = C\left[g\, m_W W^+_\mu W^{\mu-} + \frac{g}{2c_W} m_Z Z_\mu Z^\mu\right] h, \tag{A.3}$$

where a, b, and C are real, $c_W = \cos\theta_W$, and θ_W is the Weinberg angle. In the limit, $a = C = 1$, and $b = \lambda = 0$, we obtain the SM.

We use the notation for the covariant derivatives contained in Romão and Silva [52], with all etas positive, which coincides with the convention in [53]. Some relevant vertices are

$$\begin{aligned}
h\bar{\psi}\psi &\to -i\,\frac{g\,m_f}{2m_W}\,(a + ib\gamma_5)\,, \\
hH^+H^- &\to i\,\lambda\, v\,, \\
hW^{+\mu}W^{-\nu} &\to i\,g\,m_W\,C\,g^{\mu\nu}\,, \\
hZ^\mu Z^\nu &\to i\,\frac{g\,m_Z}{\cos(\theta_W)}\,C\,g^{\mu\nu}\,, \\
H^+H^-A^\mu &\to -ie\,(p_+ - p_-)^\mu\,, \\
H^+H^-Z^\mu &\to -ig\,\frac{\cos(2\theta_W)}{2\cos(\theta_W)}(p_+ - p_-)^\mu\,, \\
H^+H^-A^\mu A^\nu &\to 2i\,e^2 g^{\mu\nu}\,, \\
H^+H^-Z^\mu A^\nu &\to ieg\,\frac{\cos(2\theta_W)}{\cos(\theta_W)} g^{\mu\nu}\,.
\end{aligned} \tag{A.4}$$

These couplings were checked for the 2HDM with FeynRules [54] with the conventions of Romão and Silva [52] for positive ηs.

A.2 Tree level production and decay

In this article, we use

$$\tau = 4m^2/m_h^2, \tag{A.5}$$

where m is the mass of the relevant particle while $m_h = 125\,\text{GeV}$. This is the notation of [53]. In [20, 55, 56] the notation is $\tau(\text{theirs}) = \tau^{-1}$.

The decays into fermions are given by

$$\Gamma(h \to f\bar{f}) = N_c \frac{G_\mu\, m_f^2}{4\sqrt{2}\pi} m_h \left[a^2\beta_f^3 + b^2\beta_f\right], \tag{A.6}$$

JHEP12(2014)043

where $N_c = 3$ ($N_c = 1$) for quarks (leptons) and $\beta_f = \sqrt{1 - 4m_f^2/m_h^2} = \sqrt{1-\tau}$. The decays into two vector bosons are given by

$$\Gamma(h \to V^{(*)}V^{(*)}) = C^2\ \Gamma_{\rm SM}(h \to V^{(*)}V^{(*)}), \tag{A.7}$$

and the partial decay widths in the SM-Higgs case in the two-, three- and four-body approximations, $\Gamma_{\rm SM}(h \to V^{(*)}V^{(*)})$, can be found in section I.2.2 of ref. [55].

For the vector boson fusion (VBF) and associated (VH) productions, we find

$$\frac{\sigma_{\rm VBF}}{\sigma^{\rm SM}_{\rm VBF}} = \frac{\sigma_{\rm VH}}{\sigma^{\rm SM}_{\rm VH}} = C^2, \tag{A.8}$$

while, for the $b\bar{b}$ production,

$$\frac{\sigma(b\bar{b} \to h)}{\sigma^{\rm SM}(b\bar{b} \to h)} = a^2 + b^2. \tag{A.9}$$

We point out that the expressions shown here hold for any model with the effective Lagrangians of eqs. (A.1)–(A.3). Also, there is no interference between the scalar a couplings and the pseudoscalar b couplings in eqs. (A.6) or (A.9).

B Amplitudes for $h \to \gamma\gamma$

B.1 Fermion loop

The relevant interaction for the fermion loop is in (A.1). The one-loop amplitude reads

$$M_F^{\gamma\gamma} \equiv (q_1 \cdot q_2\, \epsilon_1 \cdot \epsilon_2 - q_1 \cdot \epsilon_2\, q_2 \cdot \epsilon_1)\, c_F^{\gamma\gamma} + \epsilon_{\mu\nu\alpha\beta}\ q_1^\mu q_2^\nu \epsilon_1^\alpha \epsilon_2^\beta\ d_F^{\gamma\gamma}\,, \tag{B.1}$$

where

$$\begin{aligned} c_F^{\gamma\gamma} &= -\frac{e^2 Q_f^2 g}{m_W}\frac{4a\, m_f^2}{m_h^2}\frac{1}{16\pi^2}\left[\left(4m_f^2 - m_h^2\right) C_0(0,0,m_h^2,m_f^2,m_f^2,m_f^2) + 2\right]\,, \\ d_F^{\gamma\gamma} &= 4\frac{e^2 Q_f^2 g}{m_W}\frac{1}{16\pi^2} b\, m_f^2\ C_0(0,0,m_h^2,m_f^2,m_f^2,m_f^2)\,, \end{aligned} \tag{B.2}$$

where C_0 is one of the Passarino-Veltman [57] scalar loop integrals. Their relation with other expressions for the one loop integrals is explained in appendix E. Note that the definition of the amplitude in eq. (B.1) is the same as in ref. [53], but differs by an irrelevant global sign from the definition in refs. [20, 55].

To make contact with the more conventional notation we define

$$c_F^{\gamma\gamma} \equiv \frac{e^2 g}{m_W}\frac{1}{16\pi^2} X_F^{\gamma\gamma}, \quad d_F^{\gamma\gamma} \equiv \frac{e^2 g}{m_W}\frac{1}{16\pi^2} Y_F^{\gamma\gamma}, \quad \tau_f \equiv \frac{4m_f^2}{m_h^2}\,. \tag{B.3}$$

We then get

$$\begin{aligned} X_F^{\gamma\gamma} &= -\frac{4a\, Q_f^2\, m_f^2}{m_h^2}\left[\left(4m_f^2 - m_h^2\right) C_0(0,0,m_h^2,m_f^2,m_f^2,m_f^2) + 2\right]\,, \\ Y_F^{\gamma\gamma} &= 4b\, Q_f^2\, m_f^2\ C_0(0,0,m_h^2,m_f^2,m_f^2,m_f^2)\,, \end{aligned} \tag{B.4}$$

JHEP12(2014)043

for each fermion f. Finally, using

$$C_0(0,0,m_h^2,m_f^2,m_f^2,m_f^2) = -\frac{\tau_f f(\tau_f)}{2m_f^2}, \tag{B.5}$$

where $f(\tau)$ is the function defined in the Higgs Hunter's Guide [53],

$$f(\tau) = \begin{cases} \left[\sin^{-1}\left(\sqrt{1/\tau}\right)\right]^2, & \text{if } \tau \geq 1\,, \\ -\frac{1}{4}\left[\ln\left(\frac{1+\sqrt{1-\tau}}{1-\sqrt{1-\tau}}\right) - i\pi\right]^2, & \text{if } \tau < 1\,, \end{cases} \tag{B.6}$$

we obtain (summing over all fermions)

$$\begin{aligned} X_F^{\gamma\gamma} &= -\sum_f N_c^f 2a\, Q_f^2\, \tau_f \left[1 + (1-\tau_f) f(\tau_f)\right], \\ Y_F^{\gamma\gamma} &= -\sum_f N_c^f 2b\, Q_f^2\, \tau_f f(\tau_f). \end{aligned} \tag{B.7}$$

B.2 Gauge boson loops

As the only modification introduced by the new Lagrangian is a multiplicative constant C, we can use the SM result ($C = 1$ in the SM). Using the same notation as in eq. (B.3), we get [53],

$$X_W^{\gamma\gamma} = C\left[2 + 3\tau_W + 3\tau_W(2-\tau_W) f(\tau_W)\right], \tag{B.8}$$

and, of course, $Y_W^{\gamma\gamma} = 0$.

B.3 Charged Higgs loops

We get for the three diagrams contributing to this process,

$$M_H^{\gamma\gamma} = (q_1 \cdot q_2\, \epsilon_1 \cdot \epsilon_2 - q_1 \cdot \epsilon_2\, q_2 \cdot \epsilon_1)\, c_H^{\gamma\gamma}, \tag{B.9}$$

where

$$c_H^{\gamma\gamma} = -\frac{4e^2\lambda v}{m_h^2 16\pi^2}\left[2m_{H^\pm}^2 C_0(0,0,m_h^2,m_{H^\pm}^2,m_{H^\pm}^2,m_{H^\pm}^2) + 1\right]. \tag{B.10}$$

In the notation of eq. (B.3) we get

$$\begin{aligned} X_H^{\gamma\gamma} &= -\frac{4\lambda m_W v}{g m_h^2}\left[2m_{H^\pm}^2 C_0(0,0,m_h^2,m_{H^\pm}^2,m_{H^\pm}^2,m_{H^\pm}^2) + 1\right] \\ &= -\frac{\lambda v^2}{2m_{H^\pm}^2}\tau_\pm\left[1 - \tau_\pm f(\tau_\pm)\right]. \end{aligned} \tag{B.11}$$

Note that this is in agreement with eq. (2.17) of ref. [53], despite the apparent sign difference, because our definition of the coupling, in eq. (A.2), also differs in sign from their eq. (2.15). So we are in complete agreement with ref. [53]. With respect to ref. [20], if we compare with their eqs. (A.8) and (A.4), again we differ by a global sign and we are, therefore, in agreement. The same holds for ref. [55].

JHEP12(2014)043

B.4 Renormalization and gauge invariance

As is well known, the loop contributions to $h \to \gamma\gamma$ should be finite and gauge invariant. This is not achieved on a diagram by diagram basis, but, rather, this should be true after adding all the diagrams. With the help of `FeynCalc` [58], we have explicitly verified this.

C Amplitudes for $h \to Z\gamma$

C.1 Fermion Loop

With the kinematics $h(p) \to Z(q_2)\gamma(q_1)$, the fermion loop yields an expression similar to the one for $h \to \gamma\gamma$:

$$M_F^{Z\gamma} = (q_1 \cdot q_2\, \epsilon_1 \cdot \epsilon_2 - q_1 \cdot \epsilon_2\, q_2 \cdot \epsilon_1)\, c^{Z\gamma} + \epsilon_{\mu\nu\alpha\beta}\, q_1^\mu q_2^\nu \epsilon_1^\alpha \epsilon_2^\beta\, d^{Z\gamma}\,. \tag{C.1}$$

Again, defining

$$c^{Z\gamma} \equiv \frac{e^2 g}{m_W}\frac{1}{16\pi^2} X_F^{Z\gamma}, \quad d^{Z\gamma} \equiv \frac{e^2 g}{m_W}\frac{1}{16\pi^2} Y_F^{Z\gamma}\,, \tag{C.2}$$

we get (summing over all the fermions)

$$\begin{aligned} X_F^{Z\gamma} &= -\sum_f N_c^f \frac{4a\, g_V^f\, Q_f\, m_f^2}{s_W c_W}\left[\frac{2m_Z^2}{(m_h^2-m_Z^2)^2}\left[B_0(m_h^2,m_f^2,m_f^2) - B_0(m_Z^2,m_f^2,m_f^2)\right]\right. \\ &\left. + \frac{1}{m_h^2-m_Z^2}\left[\left(4m_f^2 - m_h^2 + m_Z^2\right) C_0(m_Z^2,0,m_h^2,m_f^2,m_f^2,m_f^2) + 2\right]\right]\,, \end{aligned} \tag{C.3}$$

$$Y_F^{Z\gamma} = \sum_f N_c^f \frac{4b\, g_V^f\, Q_f\, m_f^2}{s_W c_W} C_0(m_Z^2,0,m_h^2,m_f^2,m_f^2,m_f^2)\,. \tag{C.4}$$

C.2 Gauge boson loops

As the only modification introduced by the new Lagrangian is a multiplicative constant C, we can use the SM result ($C = 1$ in the SM). Using the same notation as in eq. (B.3), we get

$$X_W^{Z\gamma} = \frac{C}{\tan\theta_W} I_W\,, \tag{C.5}$$

where

$$\begin{aligned} I_W &= \frac{1}{(m_h^2-m_Z^2)^2}\left[m_h^2(1-\tan^2\theta_W) - 2m_W^2(-5+\tan^2\theta_W)\right] m_Z^2 \Delta B_0 \\ &+ \frac{1}{m_h^2-m_Z^2}\left[m_h^2(1-\tan^2\theta_W) - 2m_W^2(-5+\tan^2\theta_W)\right. \\ &\left. + 2m_W^2\left[(-5+\tan^2\theta_W)(m_h^2-2M_W^2) - 2m_Z^2(-3+\tan^2\theta_W)\right] C_0\right]\,, \end{aligned} \tag{C.6}$$

with

$$\begin{aligned} \Delta B_0 &= B_0(m_h^2,m_W^2,m_W^2) - B_0(m_Z^2,m_W^2,m_W^2), \\ C_0 &= C_0(m_Z^2,0,m_h^2,m_W^2,m_W^2,m_W^2)\,, \end{aligned} \tag{C.7}$$

and, of course, $Y_W^{Z\gamma} = 0$.

JHEP12(2014)043

C.3 Charged Higgs loops

There are three diagram contributions to this process. Adding them, we get

$$M_{H^\pm}^{Z\gamma} = (q_1 \cdot q_2\, \epsilon_1 \cdot \epsilon_2 - q_1 \cdot \epsilon_2\, q_2 \cdot \epsilon_1)\, c_{H^\pm}^{Z\gamma}\,. \tag{C.8}$$

Defining, as before,

$$c_{H^\pm}^{Z\gamma} = \frac{e^2 g}{m_W} \frac{1}{16\pi^2} X_{H^\pm}^{Z\gamma}\,, \tag{C.9}$$

we get

$$X_{H^\pm}^{Z\gamma} = -\frac{1}{\tan\theta_W} \frac{\lambda v^2 (1-\tan^2\theta_W)}{m_h^2 - m_Z^2} \left[\frac{m_Z^2}{m_h^2 - m_Z^2} \Big(B_0(m_h^2, m_\pm^2, m_\pm^2) - B_0(m_Z^2, m_\pm^2, m_\pm^2) \Big) \right.$$
$$\left. + \Big(2m_\pm^2 C_0(m_Z^2, 0, m_h^2, , m_\pm^2, m_\pm^2, m_\pm^2) + 1 \Big) \right]. \tag{C.10}$$

These results agree with refs. [53, 55], except for an irrelevant global sign. See section E.2 for details.

C.4 Renormalization and gauge invariance

It is known that a counterterm in needed in order to get a finite result for this process [59]. This happens despite the fact that there is no tree level coupling $hZ\gamma$. But, as explained in ref. [59], the existence of the coupling hZZ and the renormalization of the mixing $Z\gamma$ leads to a counterterm. In that work, the authors were mainly concerned with the divergent part and did not write the full counterterm. With our conventions here[5] we should write instead of their eq. (2.16):

$$T_{Z\gamma}^{\nu\nu} = -2 \frac{e g^2 \cos\theta_W M_W}{16\pi^2} (1 + \tan^2\theta_W)\, g^{\mu\nu} B_0(0, M_W^2, M_W^2)\,, \tag{C.11}$$

where

$$B_0(0, M_W^2, M_W^2) = \Delta_\epsilon - \ln \frac{M_W^2}{\mu^2}, \quad \Delta_\epsilon = \frac{2}{\epsilon} - \gamma + \ln 4\pi\,, \tag{C.12}$$

γ is the Euler constant, and μ is the parameter introduced in dimensional regularization to correct for the fact that the electric charge is no longer dimensionless in $d \neq 4$. Apart from a global minus sign, the divergent part is precisely equal to eq. (2.16) of ref. [59]. But there is an important point here concerning the finite parts. If we do not take the counterterm as in eq. (C.11), we will not be able to cancel the dependence on the scale μ when we sum all the irreducible diagrams. We have checked this by evaluating all the reducible diagrams and showing that these sum to the counterterm, that is

$$\sum_{\text{reducible}} = -2 \frac{e g^2 \cos\theta_W M_W}{16\pi^2} (1 + \tan^2\theta_W) g^{\mu\nu} B_0(0, M_W^2, M_W^2) \equiv T_{Z\gamma}^{\nu\nu}. \tag{C.13}$$

So, in the end, we get a finite result that does not depend on the scale μ.

[5] Our Feynman rules differ from ref. [59], see ref. [52], and there is a global sign difference.

JHEP12(2014)043

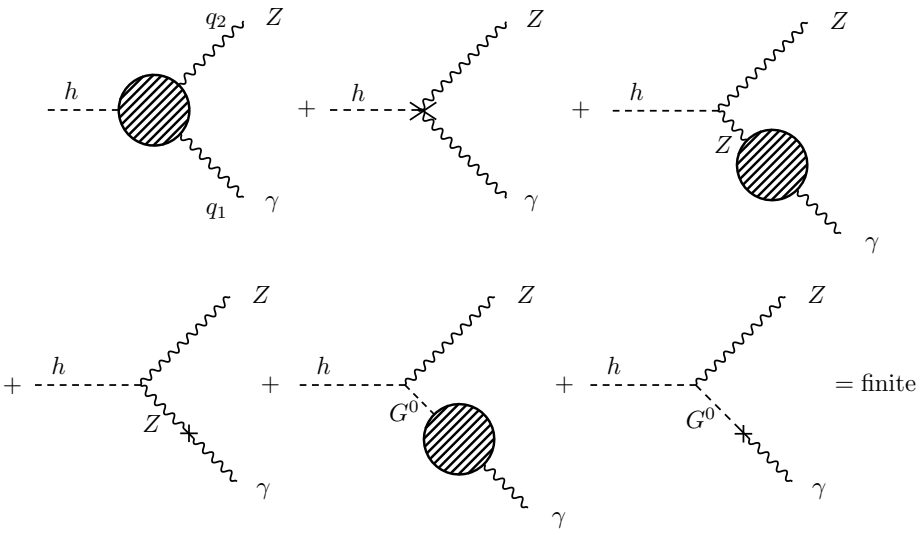

Figure 13. Classes of one loop diagrams contributing to $h \to Z\gamma$.

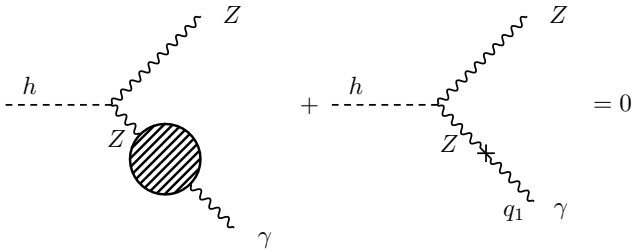

Figure 14. Sum of diagrams which vanish for a photon on mass shell.

Sometimes it is stated that to get the correct finite result for the on-shell $hZ\gamma$ three-point function all we have to do is to add to the irreducible diagrams the sum of the reducible diagrams, ignoring the counterterms. For completeness, we include here an explanation of this statement. To be precise, one should add all relevant one loop diagrams, including reducible, irreducible and counterterms, as shown in figure 13.

The last two diagrams in figure 13, which involve the Goldstone boson G^0, vanish. One may keep either of them in or exclude it at will. Moreover, the fact that we are using the on mass shell renormalization, means that the third and fourth diagrams in figure 13 add to zero, as shown diagrammatically in figure 14.

Thus, we are left with the first two diagrams in figure 13. We will now show that adding the first and third diagram in figure 13 yields the same result (as explained above, the fifth and sixth diagrams vanish and, thus, are optional). To understand this, we have to realize that the counterterm $\delta Z_{hZ\gamma}$ on the second diagram of figure 13 and the counterterm $\delta Z_{Z\gamma}$ in the photon leg on the fourth diagram of figure 13 are related. To show this, we start with the relevant part of the Lagrangian

$$\mathcal{L} = \frac{1}{8}\left(v^2 + 2vh + h^2\right)\left[g^2 W_\mu^3 W_\mu^{3\mu} + g'^2 B_\mu B^\mu - 2gg' W_\mu^3 B^\mu\right] + \cdots \tag{C.14}$$

JHEP12(2014)043

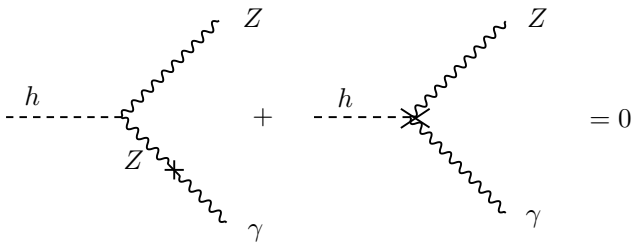

Figure 15. Diagrammatic form of evaluating the fourth diagram in figure 13 via eq. (C.19).

and perform the shifts

$$g \to g + \delta g, \quad g' \to g' + \delta g' \,. \tag{C.15}$$

After using $g' = g \tan\theta_W$ and

$$W^3_\mu = Z_\mu \cos\theta_W + A_\mu \sin\theta_W, \quad B_\mu = -Z_\mu \sin\theta_W + A_\mu \cos\theta_W, \tag{C.16}$$

we get

$$\begin{aligned} &\left[g^2 W^3_\mu W^{3\mu} + g'^2 B_\mu B^\mu - 2gg' W^3_\mu B^\mu\right] \\ &\quad \to \frac{g^2}{\cos^2\theta_W} Z_\mu Z^\mu + 2g Z_\mu Z^\mu (\delta g + \delta g' \tan^2\theta_W) + 2g Z_\mu A^\mu (\delta g \tan\theta_W - \delta g'). \end{aligned} \tag{C.17}$$

As the mixing term in $Z_\mu A^\mu$ is already first order in the corrections, we do not need to perform the shifts in v and h to get, finally,

$$\delta Z_{Z\gamma} = \frac{1}{2} v\, \delta Z_{hZ\gamma}. \tag{C.18}$$

Let us now evaluate the diagram with the counterterm in figure 14. We have, for on-shell photon ($q_1^2 = 0$),

$$i \frac{g}{\cos\theta_W} M_Z \frac{-i}{-M_Z^2}\, i\, \delta Z_{Z\gamma} \;=\; -i\, \frac{g}{M_W}\, \delta Z_{Z\gamma} = -i \delta Z_{hZ\gamma}, \tag{C.19}$$

where we have used eq. (C.18) and $M_W = \frac{1}{2} g\, v$. We obtain the result in figure 15.

Having established that the calculation can be performed exclusively with the first and second diagrams in figure 13, and combining figures 14 and 15, we obtain the result in figure 16, which we were seeking. That is: as often stated, one can add all reducible and irreducible diagrams, ignoring the counterterms.

D Widths for loop decays

The total width is given by

$$\Gamma = \frac{1}{8\pi} \frac{|\vec{q}_1|}{m_h^2} \overline{|M|^2} \,. \tag{D.1}$$

JHEP12(2014)043

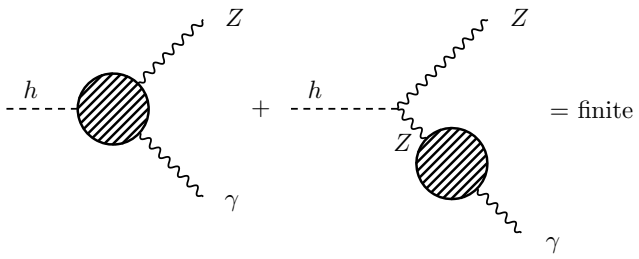

Figure 16. Diagrammatic form of evaluating the fourth diagram in figure 13 via eq. (C.19).

D.1 $h \to \gamma\gamma$

In this case, $|\vec{q}_1| = m_h/2$, and

$$\begin{aligned}\overline{|M|^2} = \left(\frac{eg}{16\pi^2 m_W}\right)^2 \Big[&|X_F^{\gamma\gamma} + X_W^{\gamma\gamma} + X_H^{\gamma\gamma}|^2 \left(q_1 \cdot q_1 g_{\mu\nu} - q_{1\mu} q_{2\nu}\right)\left(q_1 \cdot q_1 g_{\mu'\nu'} - q_{1\mu'} q_{2\nu'}\right) \\ &(-g^{\mu\mu'})(-g^{\nu\nu'}) \\ &+|Y_F^{\gamma\gamma}|^2 \, \epsilon_{\mu\nu\alpha\beta} q_1^\mu q_2^\nu \epsilon_{\mu'\nu'\alpha'\beta'} q_1^{\mu'} q_2^{\nu'} (-g^{\alpha\alpha'})(-g^{\beta\beta'})\Big] \\ = \left(\frac{eg}{16\pi^2 m_W}\right)^2 &\frac{m_h^4}{2}\left(|X_F^{\gamma\gamma} + X_W^{\gamma\gamma} + X_H^{\gamma\gamma}|^2 + |Y_F^{\gamma\gamma}|^2\right) . \end{aligned} \tag{D.2}$$

Putting everything together, and including the factor 1/2 for identical particles, we get the final result

$$\Gamma(h \to \gamma\gamma) = \frac{G_F \alpha^2 m_h^3}{128\sqrt{2}\pi^3}\left(|X_F^{\gamma\gamma} + X_W^{\gamma\gamma} + X_H^{\gamma\gamma}|^2 + |Y_F^{\gamma\gamma}|^2\right) . \tag{D.3}$$

D.2 $h \to Z\gamma$

Now, we have $|\vec{q}_1| = (m_h^2 - m_Z^2)/(2m_h)$, and

$$\begin{aligned}\overline{|M|^2} = \left(\frac{eg}{16\pi^2 m_W}\right)^2 \Big[&|X_F^{Z\gamma} + X_W^{Z\gamma} + X_H^{Z\gamma}|^2 \left(q_1 \cdot q_1 g_{\mu\nu} - q_{1\mu} q_{2\nu}\right)\left(q_1 \cdot q_1 g_{\mu'\nu'} - q_{1\mu'} q_{2\nu'}\right) \\ &(-g^{\mu\mu'})\left(-g^{\nu\nu'} + \frac{q_2^\nu q_2^{\nu'}}{m_Z^2}\right) \\ &+|Y_F^{Z\gamma}|^2 \epsilon_{\mu\nu\alpha\beta} q_1^\mu q_2^\nu \epsilon_{\mu'\nu'\alpha'\beta'} q_1^{\mu'} q_2^{\nu'} (-g^{\alpha\alpha'})\left(-g^{\beta\beta'} + \frac{q_2^\beta q_2^{\beta'}}{m_Z^2}\right)\Big] \\ = \left(\frac{eg}{16\pi^2 m_W}\right)^2 &\frac{(m_h^2 - m_Z^2)^2}{2}\left(|X_F^{Z\gamma} + X_W^{Z\gamma} + X_H^{Z\gamma}|^2 + |Y_F^{Z\gamma}|^2\right) , \end{aligned} \tag{D.4}$$

and, for the final width,

$$\Gamma(h \to Z\gamma) = \frac{G_F \alpha^2 m_h^3}{64\sqrt{2}\pi^3}\left(1 - \frac{m_Z^2}{m_h^2}\right)^3 \left(|X_F^{Z\gamma} + X_W^{Z\gamma} + X_H^{Z\gamma}|^2 + |Y_F^{Z\gamma}|^2\right) . \tag{D.5}$$

JHEP12(2014)043

E Relation between the Passarino-Veltman functions and other loop functions

When we compute the one-loop diagrams, as we did, using `FeynCalc` [58], the result is naturally presented in terms of the well-known Passarino-Veltman integrals [57]. These are in general complicated functions of the external momenta and masses and usually only possible to be expressed in terms of very complicated functions. Normally it is better to evaluate them numerically and for that there is the package `LoopTools` [60, 61]. However for special situations, like zero external momenta or equal masses in the loops, these loop integrals have simpler forms and can be expressed in terms of simple functions. This is the case for the loops studied here and we present in this appendix the relations of these Passarino-Veltman integrals with other representations found in the literature.

E.1 The integrals for $h \to \gamma\gamma$

In this decay, all results can be expressed in terms of the Passarino-Veltman integral $C_0(0,0,m_h^2,m^2,m^2,m^2)$, where m is the mass of the particle running in the loop. We have already given in eq. (B.5) the relation with the function $f(\tau)$ defined in the Higgs Hunter's Guide [53],

$$C_0(0,0,m_h^2,m^2,m^2,m^2) = -\frac{\tau f(\tau)}{2m^2}, \quad \tau = \frac{4m^2}{m_h^2}, \tag{E.1}$$

where $f(\tau)$ is defined in eq. (B.6).

E.2 The integrals for $h \to Z\gamma$

In the Higgs Hunter's Guide [53], a different set of integrals, $I_1(a,b)$ and $I_2(a,b)$ were introduced. They are defined as follows:

$$I_1(a,b) = \frac{ab}{2(a-b)} + \frac{a^2b^2}{2(a-b)^2}\Big[f(a)-f(b)\Big] + \frac{a^2b}{(a-b)^2}\Big[g(a)-g(b)\Big]\,, \tag{E.2}$$

$$I_2(a,b) = -\frac{ab}{2(a-b)}\Big[f(a)-f(b)\Big]\,, \tag{E.3}$$

where $f(\tau)$ was defined in eq. (B.6), and $g(\tau)$ is given by

$$g(\tau) = \begin{cases} \sqrt{\tau-1}\ \sin^{-1}\left(\sqrt{1/\tau}\right), & \text{if } \tau \geq 1\,, \\ \frac{1}{2}\sqrt{1-\tau}\ \left[\ln\left(\dfrac{1+\sqrt{1-\tau}}{1-\sqrt{1-\tau}}\right) - i\pi\right], & \text{if } \tau < 1\,. \end{cases} \tag{E.4}$$

Comparing their results with our results and those of ref. [59], we get

$$I_1(\tau,\lambda) = 4J_2(\beta_Z,\beta_H), \quad I_2(\tau,\lambda) = J_1(\beta_Z,\beta_H)\,, \tag{E.5}$$

where

$$\tau = \frac{4m^2}{m_h^2}, \quad \lambda = \frac{4m^2}{m_Z^2}, \quad \beta_Z = \frac{m_Z^2}{m^2}, \quad \beta_H = \frac{m_H^2}{m^2}\,, \tag{E.6}$$

JHEP12(2014)043

and m is any mass running in the loops. Again, we have numerically checked that these relations hold for any value of the arguments.

To compare our results in terms of the Passarino-Veltman functions with those of ref. [53], we notice that

$$C_0(m_Z^2, 0, m_h^2, m^2, m^2, m^2) = -\frac{1}{m^2} I_2(\tau, \lambda)\,, \tag{E.7}$$

$$\Delta B_0 = -\frac{m_h^2 - m_Z^2}{m_Z^2} - \frac{(m_h^2 - m_Z^2)^2}{2m^2 m_Z^2}\, I_1(\tau, \lambda) + 2\,\frac{m_h^2 - m_Z^2}{m_Z^2}\, I_2(\tau, \lambda)\,. \tag{E.8}$$

We have checked these equations numerically with the help of the package `LoopTools` [60, 61].

Using these relations, one can check that our eqs. (C.3), (C.6) and (C.10) agree with eqs. (C.12), (C.13) and (C.14) of ref. [53] up to an overall sign. We notice that our coupling to the charged Higgs translate into their notation

$$\lambda v \to -R^h_{H^\pm}\,. \tag{E.9}$$

There is no equivalent result to our eq. (C.4) in ref. [53], but we are in agreement with ref. [55] up to global signs. However we warn the reader that the definitions of I_1, I_2 and $g(\tau)$ in eqs. (2.55) and (2.56) of ref. [55] are not consistent.

F Production and decay involving gluons

Relating with the expression for the $\gamma\gamma$ decay, we find

$$\Gamma(h \to gg) = \frac{G_F \alpha_S^2 m_h^3}{64\sqrt{2}\pi^3} \left(|X_F^{gg}|^2 + |Y_F^{gg}|^2\right)\,, \tag{F.1}$$

where

$$\begin{aligned} X_F^{gg} &= -\sum_q 2a_q\,\tau_q\,[1 + (1-\tau_q) f(\tau_q)]\,, \\ Y_F^{gg} &= -\sum_q 2b_q\,\tau_q f(\tau_q)\,, \end{aligned} \tag{F.2}$$

and the sums run only over quarks q.

Similarly,

$$\sigma(gg \to h) = \frac{G_\mu \alpha_s^2}{512\sqrt{2}\pi} \left(|X_F^{gg}|^2 + |Y_F^{gg}|^2\right)\,. \tag{F.3}$$

These are dominated by the triangle with top quark in the loop, and, depending on $\tan\beta$, also by the triangle with bottom quark in the loop. Thus, we can use

$$\frac{\sigma(gg \to h)}{\sigma^{\rm SM}(gg \to h)} = \frac{|a_t\, A_{1/2}(\tau_t) + a_b\, A_{1/2}(\tau_b)|^2 + |b_t\, A^A_{1/2}(\tau_t) + b_b\, A^A_{1/2}(\tau_b)|^2}{|A_{1/2}(\tau_t) + A_{1/2}(\tau_b)|^2}\,, \tag{F.4}$$

where

$$\begin{aligned} A_{1/2}(\tau_q) &= = 2\tau_q\,[1 + (1-\tau_q) f(\tau_q)]\,, \\ A^A_{1/2}(\tau_q) &= 2\tau_q f(\tau_q)\,. \end{aligned} \tag{F.5}$$

JHEP12(2014)043

Acknowledgments

We are grateful to Rui Santos for many discussions related to the Higgs production channels and to Augusto Barroso for discussions on the renormalization of the $hZ\gamma$ vertex. This work was partially supported by FCT — *Fundação para a Ciência e a Tecnologia*, under the projects PEst-OE/FIS/UI0777/2013 and CERN/FP/123580/2011. D. F. is also supported by FCT under the project EXPL/FIS-NUC/0460/2013.

References

[1] ATLAS collaboration, *Observation of a new particle in the search for the Standard Model Higgs boson with the ATLAS detector at the LHC*, *Phys. Lett.* **B 716** (2012) 1 [arXiv:1207.7214] [INSPIRE].

[2] CMS collaboration, *Observation of a new boson at a mass of 125 GeV with the CMS experiment at the LHC*, *Phys. Lett.* **B 716** (2012) 30 [arXiv:1207.7235] [INSPIRE].

[3] CMS collaboration, *Search for the standard model Higgs boson produced in association with a W or a Z boson and decaying to bottom quarks*, *Phys. Rev.* **D 89** (2014) 012003 [arXiv:1310.3687] [INSPIRE].

[4] CDF and D0 collaborations, B. Tuchming, *Higgs boson production and properties at the Tevatron*, arXiv:1405.5058 [INSPIRE].

[5] ATLAS collaboration, https://twiki.cern.ch/twiki/bin/view/AtlasPublic/HiggsPublicResults.

[6] CMS Collaboration, https://twiki.cern.ch/twiki/bin/view/CMSPublic/PhysicsResultsHIG.

[7] ATLAS collaboration, *Search for Higgs boson decays to a photon and a Z boson in pp collisions at $\sqrt{s} = 7$ and 8 TeV with the ATLAS detector*, *Phys. Lett.* **B 732** (2014) 8 [arXiv:1402.3051] [INSPIRE].

[8] CMS collaboration, *Search for a Higgs boson decaying into a Z and a photon in pp collisions at $\sqrt{s} = 7$ and 8 TeV*, *Phys. Lett.* **B 726** (2013) 587 [arXiv:1307.5515] [INSPIRE].

[9] CMS collaboration, *Study of the Mass and Spin-Parity of the Higgs Boson Candidate Via Its Decays to Z Boson Pairs*, *Phys. Rev. Lett.* **110** (2013) 081803 [arXiv:1212.6639] [INSPIRE].

[10] ATLAS collaboration, *Studies of Higgs spin and parity with the ATLAS detector at the LHC*, PoS(EPS-HEP 2013)125.

[11] G.C. Branco et al., *Theory and phenomenology of two-Higgs-doublet models*, *Phys. Rept.* **516** (2012) 1 [arXiv:1106.0034] [INSPIRE].

[12] I.F. Ginzburg, M. Krawczyk and P. Osland, *Two Higgs doublet models with CP-violation*, hep-ph/0211371 [INSPIRE].

[13] W. Khater and P. Osland, *CP violation in top quark production at the LHC and two Higgs doublet models*, *Nucl. Phys.* **B 661** (2003) 209 [hep-ph/0302004] [INSPIRE].

JHEP12(2014)043

[14] A.W. El Kaffas, P. Osland and O.M. Ogreid, *CP violation, stability and unitarity of the two Higgs doublet model*, *Nonlin. Phenom. Complex Syst.* **10** (2007) 347 [hep-ph/0702097] [INSPIRE].

[15] A.W. El Kaffas, W. Khater, O.M. Ogreid and P. Osland, *Consistency of the two Higgs doublet model and CP-violation in top production at the LHC*, *Nucl. Phys.* **B 775** (2007) 45 [hep-ph/0605142] [INSPIRE].

[16] A. Wahab El Kaffas, P. Osland and O.M. Ogreid, *Constraining the Two-Higgs-Doublet-Model parameter space*, *Phys. Rev.* **D 76** (2007) 095001 [arXiv:0706.2997] [INSPIRE].

[17] P. Osland, P.N. Pandita and L. Selbuz, *Trilinear Higgs couplings in the two Higgs doublet model with CP-violation*, *Phys. Rev.* **D 78** (2008) 015003 [arXiv:0802.0060] [INSPIRE].

[18] B. Grzadkowski and P. Osland, *Tempered Two-Higgs-Doublet Model*, *Phys. Rev.* **D 82** (2010) 125026 [arXiv:0910.4068] [INSPIRE].

[19] A. Arhrib, E. Christova, H. Eberl and E. Ginina, *CP violation in charged Higgs production and decays in the Complex Two Higgs Doublet Model*, *JHEP* **04** (2011) 089 [arXiv:1011.6560] [INSPIRE].

[20] A. Barroso, P.M. Ferreira, R. Santos and J.P. Silva, *Probing the scalar-pseudoscalar mixing in the 125 GeV Higgs particle with current data*, *Phys. Rev.* **D 86** (2012) 015022 [arXiv:1205.4247] [INSPIRE].

[21] L. Lavoura and J.P. Silva, *Fundamental CP-violating quantities in a* SU(2) × U(1) *model with many Higgs doublets*, *Phys. Rev.* **D 50** (1994) 4619 [hep-ph/9404276] [INSPIRE].

[22] F.J. Botella and J.P. Silva, *Jarlskog-like invariants for theories with scalars and fermions*, *Phys. Rev.* **D 51** (1995) 3870 [hep-ph/9411288] [INSPIRE].

[23] H.E. Haber and H.E. Logan, *Radiative corrections to the $Zb\bar{b}$ vertex and constraints on extended Higgs sectors*, *Phys. Rev.* **D 62** (2000) 015011 [hep-ph/9909335] [INSPIRE].

[24] M. Baak et al., *Updated Status of the Global Electroweak Fit and Constraints on New Physics*, *Eur. Phys. J.* **C 72** (2012) 2003 [arXiv:1107.0975] [INSPIRE].

[25] T. Hermann, M. Misiak and M. Steinhauser, *$\bar{B} \to X_s\gamma$ in the Two Higgs Doublet Model up to Next-to-Next-to-Leading Order in QCD*, *JHEP* **11** (2012) 036 [arXiv:1208.2788] [INSPIRE].

[26] F. Mahmoudi, talk given at *Prospects For Charged Higgs Discovery At Colliders (CHARGED 2012)*, Uppsala, Sweden, October 8–11 2012.

[27] ATLAS collaboration, *Search for charged Higgs bosons decaying via $H^+ \to \tau\nu$ in top quark pair events using pp collision data at $\sqrt{s} = 7$ TeV with the ATLAS detector*, *JHEP* **06** (2012) 039 [arXiv:1204.2760] [INSPIRE].

[28] CMS collaboration, *Search for a light charged Higgs boson in top quark decays in pp collisions at $\sqrt{s} = 7$ TeV*, *JHEP* **07** (2012) 143 [arXiv:1205.5736] [INSPIRE].

[29] P.M. Ferreira, J.F. Gunion, H.E. Haber and R. Santos, *Probing wrong-sign Yukawa couplings at the LHC and a future linear collider*, *Phys. Rev.* **D 89** (2014) 115003 [arXiv:1403.4736] [INSPIRE].

[30] D. Fontes, J.C. Romão and J.P. Silva, *A reappraisal of the wrong-sign $hb\bar{b}$ coupling and the study of $h \to Z\gamma$*, *Phys. Rev.* **D 90** (2014) 015021 [arXiv:1406.6080] [INSPIRE].

[31] N.G. Deshpande and E. Ma, *Pattern of Symmetry Breaking with Two Higgs Doublets*, *Phys. Rev.* **D 18** (1978) 2574 [INSPIRE].

JHEP12(2014)043

[32] S. Kanemura, T. Kubota and E. Takasugi, *Lee-Quigg-Thacker bounds for Higgs boson masses in a two doublet model*, *Phys. Lett.* **B 313** (1993) 155 [hep-ph/9303263] [INSPIRE].

[33] A.G. Akeroyd, A. Arhrib and E.-M. Naimi, *Note on tree level unitarity in the general two Higgs doublet model*, *Phys. Lett.* **B 490** (2000) 119 [hep-ph/0006035] [INSPIRE].

[34] I.F. Ginzburg and I.P. Ivanov, *Tree level unitarity constraints in the 2HDM with CP-violation*, hep-ph/0312374 [INSPIRE].

[35] W. Grimus, L. Lavoura, O.M. Ogreid and P. Osland, *The oblique parameters in multi-Higgs-doublet models*, *Nucl. Phys.* **B 801** (2008) 81 [arXiv:0802.4353] [INSPIRE].

[36] M. Baak et al., *The Electroweak Fit of the Standard Model after the Discovery of a New Boson at the LHC*, *Eur. Phys. J.* **C 72** (2012) 2205 [arXiv:1209.2716] [INSPIRE].

[37] M. Spira, *HIGLU: A program for the calculation of the total Higgs production cross-section at hadron colliders via gluon fusion including QCD corrections*, hep-ph/9510347 [INSPIRE].

[38] R.V. Harlander, S. Liebler and H. Mantler, *SusHi: A program for the calculation of Higgs production in gluon fusion and bottom-quark annihilation in the Standard Model and the MSSM*, *Computer Physics Communications* **184** (2013) 1605 [arXiv:1212.3249] [INSPIRE].

[39] https://twiki.cern.ch/twiki/bin/view/LHCPhysics/Cross sections figures.

[40] ATLAS collaboration, *Physics of the Brout-Englert-Higgs boson in ATLAS*, talk given at *ICHEP2014*, Valencia, Spain, July 2–9 2014.

[41] CMS collaboration, *Physics of the Brout-Englert-Higgs boson in CMS*, talk given at *ICHEP2014*, Valencia, Spain, July 2–9 2014.

[42] D. Carmi, A. Falkowski, E. Kuflik and T. Volansky, *Interpreting LHC Higgs Results from Natural New Physics Perspective*, *JHEP* **07** (2012) 136 [arXiv:1202.3144] [INSPIRE].

[43] C.-W. Chiang and K. Yagyu, *Implications of Higgs boson search data on the two-Higgs doublet models with a softly broken Z_2 symmetry*, *JHEP* **07** (2013) 160 [arXiv:1303.0168] [INSPIRE].

[44] A. Barroso, P.M. Ferreira, R. Santos, M. Sher and J.P. Silva, *2HDM at the LHC — the story so far*, arXiv:1304.5225 [INSPIRE].

[45] ACME collaboration, J. Baron et al., *Order of Magnitude Smaller Limit on the Electric Dipole Moment of the Electron*, *Science* **343** (2014) 269 [arXiv:1310.7534] [INSPIRE].

[46] A.J. Buras, G. Isidori and P. Paradisi, *EDMs versus CPV in $B_{s,d}$ mixing in two Higgs doublet models with MFV*, *Phys. Lett.* **B 694** (2011) 402 [arXiv:1007.5291] [INSPIRE].

[47] J.M. Cline, K. Kainulainen and M. Trott, *Electroweak Baryogenesis in Two Higgs Doublet Models and B meson anomalies*, *JHEP* **11** (2011) 089 [arXiv:1107.3559] [INSPIRE].

[48] M. Jung and A. Pich, *Electric Dipole Moments in Two-Higgs-Doublet Models*, *JHEP* **04** (2014) 076 [arXiv:1308.6283] [INSPIRE].

[49] J. Shu and Y. Zhang, *Impact of a CP-violating Higgs Sector: From LHC to Baryogenesis*, *Phys. Rev. Lett.* **111** (2013) 091801 [arXiv:1304.0773] [INSPIRE].

[50] S. Inoue, M.J. Ramsey-Musolf and Y. Zhang, *CPV Phenomenology of Flavor Conserving Two Higgs Doublet Models*, *Phys. Rev.* **D 89** (2014) 115023 [arXiv:1403.4257] [INSPIRE].

[51] T. Abe, J. Hisano, T. Kitahara and K. Tobioka, *Gauge invariant Barr-Zee type contributions*

JHEP12(2014)043

to fermionic EDMs in the two-Higgs doublet models, *JHEP* **01** (2014) 106 [arXiv:1311.4704] [INSPIRE].

[52] J.C. Romao and J.P. Silva, *A resource for signs and Feynman diagrams of the Standard Model*, *Int. J. Mod. Phys.* **A 27** (2012) 1230025 [arXiv:1209.6213] [INSPIRE].

[53] J.F. Gunion, H.E. Haber, G.L. Kane and S. Dawson, *The Higgs Hunter's Guide*, *Front. Phys.* **80** (2000) 1.

[54] A. Alloul, N.D. Christensen, C. Degrande, C. Duhr and B. Fuks, *FeynRules 2.0 — A complete toolbox for tree-level phenomenology*, *Comput. Phys. Commun.* **185** (2014) 2250 [arXiv:1310.1921] [INSPIRE].

[55] A. Djouadi, *The Anatomy of electro-weak symmetry breaking. I: The Higgs boson in the standard model*, *Phys. Rept.* **457** (2008) 1 [hep-ph/0503172] [INSPIRE].

[56] A. Djouadi, *The anatomy of electro-weak symmetry breaking. II. The Higgs bosons in the minimal supersymmetric model*, *Phys. Rept.* **459** (2008) 1 [hep-ph/0503173] [INSPIRE].

[57] G. Passarino and M.J.G. Veltman, *One Loop Corrections for e^+e^- Annihilation Into $\mu^+\mu^-$ in the Weinberg Model*, *Nucl. Phys.* **B 160** (1979) 151 [INSPIRE].

[58] R. Mertig, M. Böhm and A. Denner, *Feyn Calc – Computer algebraic calculation of Feynman amplitudes*, *Comput. Phys. Commun.* **64** (1991) 345 [INSPIRE].

[59] A. Barroso, J. Pulido and J.C. Romao, *Higgs production at e^+e^- colliders*, *Nucl. Phys.* **B 267** (1986) 509 [INSPIRE].

[60] T. Hahn and M. Pérez-Victoria, *Automatized one loop calculations in four-dimensions and D-dimensions*, *Comput. Phys. Commun.* **118** (1999) 153 [hep-ph/9807565] [INSPIRE].

[61] http://www.feynarts.de/looptools.

JHEP12(2014)043